Supercooling and Freezing of HNO_3/H_2O Aerosols

by

Dustin Dickens

A thesis
presented to the University of Waterloo
in fulfilment of the
thesis requirement for the degree of
Master of Science
in
chemistry

Waterloo, Ontario Canada, 2000

I hereby declare that I am the sole author of this thesis. This is a true copy of the thesis, including any required final revisions, as accepted by my examiners.

I understand that my thesis may be made electronically available to the public.

Abstract

The freezing kinetics of binary nitric acid/water aerosols is of fundamental importance to the modelling of polar stratospheric clouds and the role they in ozone depletion over the Arctic/Antarctic regions. Cirrus clouds are also often composed of nitric acid solutions, hence an understanding of freezing process in these aerosols also aids in modelling the earth's radiation budget and global warming. This thesis explores the kinetic phase diagram of nitric acid/water aerosols with sizes ranging between 0.2 and 1.5 μm in radius and concentrations ranging between pure water and 0.45 mole fraction HNO_3. Although the kinetic phase diagram has now been studied between 0.46 mole fraction HNO_3 and pure water, more data is needed in the region between 0.18 and 0.25 mole fraction HNO_3 to confirm the results reported.

The project described in this thesis are a continuation of a project begun by Allan Bertram. The measurements involving aerosols with compositions greater than 0.25 mole fraction HNO_3 were carried out as part of Allan Bertram's Ph.D. thesis (see ref. 20) These data were later examined using a more comprehensive data analysis method (as presented in this thesis) in an effort to obtain a more complete understanding of this system.

Acknowledgements

I would like to thank:

Jim Sloan for his continued guidance, support and encouragement throughout this project.

Allan Bertram for getting me started and being very patient with me while I was learning how to not break everything around me.

Douglas Weir, Jenning Seto and Randall Skelton for computer assistance and reminding me that I am a scientist, not a plumber.

Qing Xu, Naila Siddique, and the other members of the Sloan Group (past and present) for their help, support and friendship.

All of the other people whose names have escaped me at this time. You know who you are.

Table of Contents

List of Figures

List of Abbreviations and Terms

Anneal	The process of warming the sample after nucleation to encourage crystal growth
Ice	Solid H_2O (also referred to as water ice)
PSC	Polar Stratospheric Cloud
Mountain Lee Waves	Cooling of air due to altitude changes as air passes over mountains (also called Gravity Waves or Orographic Waves)
NAD	Nitric Acid Dihydrate
NAM	Nitric Acid Monohydrate
NAT	Nitric Acid Trihydrate

1 Introduction

1.1 Creation and Destruction of Polar Ozone

The Chapman mechanism is a model describing the creation and destruction of ozone in the lower stratosphere through a cycle of simple reactions involving the photo-dissociation of oxygen, and the subsequent reactions of these lone oxygen atoms with oxygen molecules. These reactions are given in equation 1.1, where M is usually O_2 or N_2.

$$\begin{aligned} O_2 &\xrightarrow{h\nu} O + O \\ O + O_2 + M &\longrightarrow O_3 + M \\ O_3 &\xrightarrow{h\nu} O_2 + O \\ O_3 + O &\longrightarrow O_2 + O_2 \end{aligned} \qquad (1.1)$$

However, it was found that the Chapman mechanism overestimated the amount of ozone that should be present in the stratosphere. The predicted ozone concentrations were improved by considering the catalytic action of certain trace gases also present in the stratosphere. These compounds served as catalysts in the destruction of ozone molecules[1]. In 1974 Rowland and Molina proposed a gas phase cycle involving chlorine atoms[2]. Until recently, most of the work done on ozone depletion focused on these gas phase processes. It is now known that heterogeneous processes involving polar stratospheric clouds carry an important link to polar ozone depletion.

1.2 Stratospheric Aerosols and Polar Stratospheric Clouds

Sulphate aerosols have been observed in the stratosphere in the form of 60-80 wt% sulphuric acid. At temperatures which are typical for the polar regions of the stratosphere (190-200 K), sulphate aerosols will absorb water, as well as nitric acid vapour[3]. These particles are labeled type I polar stratospheric clouds (PSCs). Type Ia

PSCs are believed to consist of nonspherical crystalline particles, while type Ib PSCs are believed to consist of spherical, liquid particles[4]. Aerosols containing pure water have also been observed in the stratosphere. Clouds composed of pure water aerosols are labeled type II PSCs[5].

1.3 The Importance of PSCs to the Ozone Layer

Chlorine and bromine radicals rapidly catalyze reactions that convert ozone back to molecular oxygen. Reactive radicals can be created by the photolysis of compounds such as Cl_2, HOCl, HOBr, and Br_2[6]. These compounds can be formed by heterogeneous reactions of relatively inert reservoir species such as the following:[7]

$$\begin{aligned} ClONO_{2(g)} + HCl_{(g)} &\xrightarrow{PSC} Cl_{2(g)} + HNO_{3(l)} \\ ClONO_{2(g)} + H_2O_{(g)} &\xrightarrow{PSC} HOCl_{(g)} + HNO_{3(l)} \\ HOCl_{(g)} + HCl_{(g)} &\xrightarrow{PSC} Cl_{2(g)} + H_2O_{(l)} \end{aligned} \qquad (1.2)$$

This process is referred to as chlorine activation.

In addition, PSCs remove nitrate compounds such as N_2O_5 from the stratosphere. These compounds would normally convert reactive species back into reservoir compounds. The mechanism for this removal is:
The resulting HNO_3 is removed from the gas phase by the growing PSC particles.

$$N_2O_{5(g)} + H_2O_{(g)} \longrightarrow 2HNO_{3(g)} \qquad (1.3)$$

These particles will eventually settle due to gravity and be removed from the lower stratosphere. This process is known as denitrification.[8]

Although type II PSC particles have the highest chlorine activation rate, type I PSCs are more common, as well as tending to be smaller, hence there is far more type I PSC surface on which chlorine activation can occur.[9] Temperatures below the ice frost

point are needed for the formation of type II PSCs (<189K at 55 mbar). These temperatures routinely occur in the Antarctic stratosphere in winter and early spring. In the arctic stratosphere temperatures tend to be warmer and the ice frost point is rarely reached, except for short periods of time generally during the occurrence of mountain lee waves[10] which induce adiabatic cooling as air parcels change altitude while passing over mountain ranges[11]. Temperature fluctuations in this range could lead to changes composition and phase of aerosol particles. This cycle is complicated even more by the tendency of aerosol particles to remain liquid at temperatures below the equilibrium freezing point. The asymmetry in freezing and melting temperatures should cause a difference of up to 30 K between the formation and melting temperatures of these aerosols, for which there is some evidence in the Arctic winter stratosphere[12].

1.4 Cirrus clouds

Nitric acid solutions are also a major component of cirrus clouds. Cirrus clouds play an important role in the earth's radiation budget, which dictates global warming and cooling. Cirrus clouds reflect solar radiation, thereby cooling the earth by reducing the amount of radiation that strikes the surface.

When ultraviolet and visible wavelength radiation strikes the surface of the earth, it is converted to infrared radiation and radiated back into space. Cirrus clouds will absorb this energy at the warm cloud bottoms and emit it back into space from the cool cloud tops. Some of the heat is thus kept in the atmosphere, in much the same way as greenhouse gases such as CO_2 serve to trap heat in the lower atmosphere.

The heating effect is nearly cancelled by the cooling effect, creating a delicate balance. Still, the net observed effect is four times larger than is expected from doubling the amount of CO_2 present in the atmosphere.

How these two competing effects of clouds vary with cloud type or structure is not well understood but both are estimated to be roughly ten times as large as for a CO_2 doubling. Because radiative properties of cirrus cloud particles depend upon the structure, composition and phase of the clouds themselves, an understanding of the freezing dynamics of these particles is fundamental to the development of an adequate model for their behavior and its effect upon the radiation budget for the earth.

1.5 Freezing Kinetics

Using thermodynamics, we are able to identify the most stable phase of a substance under a given set of conditions. Supercooled liquids, however, can exist at temperatures substantially below the point at which thermodynamics indicates the bulk material should be solid. Freezing is a kinetic process that is governed by statistics. (See below.) Given enough time, all substances will freeze at any temperature below their equilibrium melting point. However, the time required for very small samples, such as aerosol particles, may be quite prolonged. For example, the equilibrium freezing point for pure water is 273K. However, supercooled water droplets have been observed in the atmosphere at temperatures as low as 233 K. The reason for this substantial supercooling can be explained by examining the kinetics of the freezing process[13].

Freezing can be considered as the occurrence of two events: nucleation and crystal growth.

Homogeneous Nucleation:

$$liquid \xrightarrow{J} liquid + nucleus \qquad (1.4)$$

Crystal Growth:

$$liquid + nucleus \xrightarrow{u} crystal \qquad (1.5)$$

where J is the kinetic rate constant for homogeneous nucleation and u is the rate for the crystal growth process. These rate processes are independent and are not necessarily both fast at a given temperature.

1.6 Homogeneous Nucleation

In order for a crystal to form from a liquid material, a nucleus must form on which the crystal lattice grows. In the case of heterogeneous nucleation, a grain of dust, an ion, or any other foreign object may act as a centre for crystal growth. There is still some debate regarding the importance of these processes in the stratosphere[14]. Currently, research has focused primarily on nucleation caused by homogeneous processes because the stratosphere is a relatively clean environment.

When a crystal forms, there is a decrease in the free energy of the droplet, ΔG, per mole of liquid that crystalizes. The decrease in the free energy upon forming a spherical crystalline region with radius r is given by $4\pi r^3 \Delta G/3V_m$, where V_m is the molar volume. There is also a surface energy associated with the interface between the crystal and the surrounding liquid. The free energy change associated with creation of this interface is $4\pi r^2 \sigma$, where σ is the surface energy per unit area. Thus, the total free energy associated with nucleus formation (W) is the sum of these terms.[15,16]

$$W = \frac{4\pi r^3 \Delta G}{3V_m} + 4\pi r^2 \sigma \qquad (1.6)$$

When r is less than r^* (see figure 1.1), W increases with r. Thus, if a crystalline region with a radius less than r^* forms, it is more favorable for the nucleus to re-melt than for crystal growth to occur. A stable nucleus is formed only when it attains a radius greater than r^*. This is the point at which the volume term, which is negative because ΔG is negative, becomes greater in magnitude than the surface energy term. Because this event is associated with an increase in free energy, it is a relatively rare occurrence, especially in small samples such as aerosol particles whose volumes are on the order of 10^{-17} litres. Once a nucleus of critical size does form however, growth of the crystal will result in a decrease in free energy.

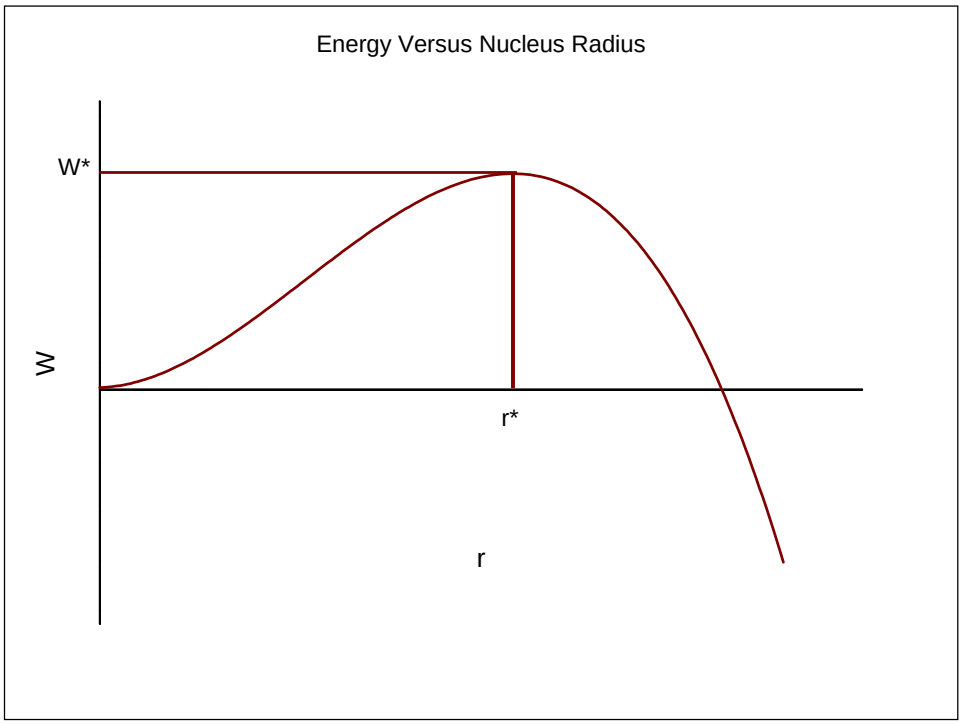

Figure 1.1
Free energy of nucleus formation as a function of nuclear radius

The probability of a thermal fluctuation leading to a sufficient increase in free energy for formation of a nucleus with a size greater than r^* is given by the Boltzmann equation[15]

$$p(W^*) \propto e^{\frac{-W^*}{RT}} \tag{1.7}$$

where R is the ideal gas constant. Formation of a nucleus also requires the rearrangement of molecules in order to form the crystalline structure. This process has an associated rate proportional to $e^{\frac{-\Delta G_D}{RT}}$, where ΔG_D is the activation energy for this rearrangement process.[16] Note also that ΔG_D is also temperature dependent. Thus, the total rate of nucleation is given by:

$$J \propto e^{\frac{-W^*}{RT}} e^{\frac{-\Delta G_D}{RT}} \tag{1.8}$$

where J is typically in units of $cm^{-3}s^{-1}$.

1.7 Crystal Growth Kinetics

Once a nucleus has been formed, either by the homogeneous process described above, or by some heterogeneous process, it becomes energetically favourable for the crystal to grow. A theoretical analysis of the mechanisms involved in crystal growth leads to equation 1.8, which describes the growth rate of the nucleus:[15,17]
where u is typically expressed in cm s^{-1}. ΔG is the decrease in free energy per mole

$$u = a_0 \nu e^{\frac{-\Delta G'}{RT}} \left(1 - e^{\frac{\Delta G}{RT}} \right) \tag{1.9}$$

when the liquid crystallizes, $\Delta G'$ is the temperature dependant activation energy for a molecule to detach from the liquid phase in order to become part of the crystal, a_0 is the intermolecular distance, and ν is the frequency of thermal vibrations within the material.

1.8 Combined effects of nucleation and crystal growth rates

In order to achieve measurable crystal formation, both processes discussed above must occur to a substantial degree. The amount of crystal formation required will be discussed in chapter 3. Because nucleation and crystal growth have different temperature dependent rates, cases can arise where one of the processes is not kinetically significant over the temperature range for which other process is fast. Examples of both situations are given in figure 1.2. In 1.2 (a), nucleation and crystal growth are both substantial at temperatures around T_m, while in figure 1.2 (b) there is no temperature at which both processes are significant. Both situations can occur in nitric acid/water aerosols[18,19], and the amount of overlap in the temperature domain between the nucleation and crystal growth curves is an important factor in determining the formation mechanisms of aerosols both in the atmosphere and in the experiments described in this thesis.

1.9 Importance of Laboratory Measurements

The measurements described in this thesis should provide atmospheric chemists with a deeper understanding of the physical properties of the particulates that reside in the upper troposphere and lower stratosphere. This understanding can be used to better model the freezing processes in the environment and determine the full impact these particles have on ozone depletion.

With the impending launch of satellites equipped with broad-band infrared instruments, the data discussed in this thesis will become an important tool for making sense of spectra collected in the stratosphere.

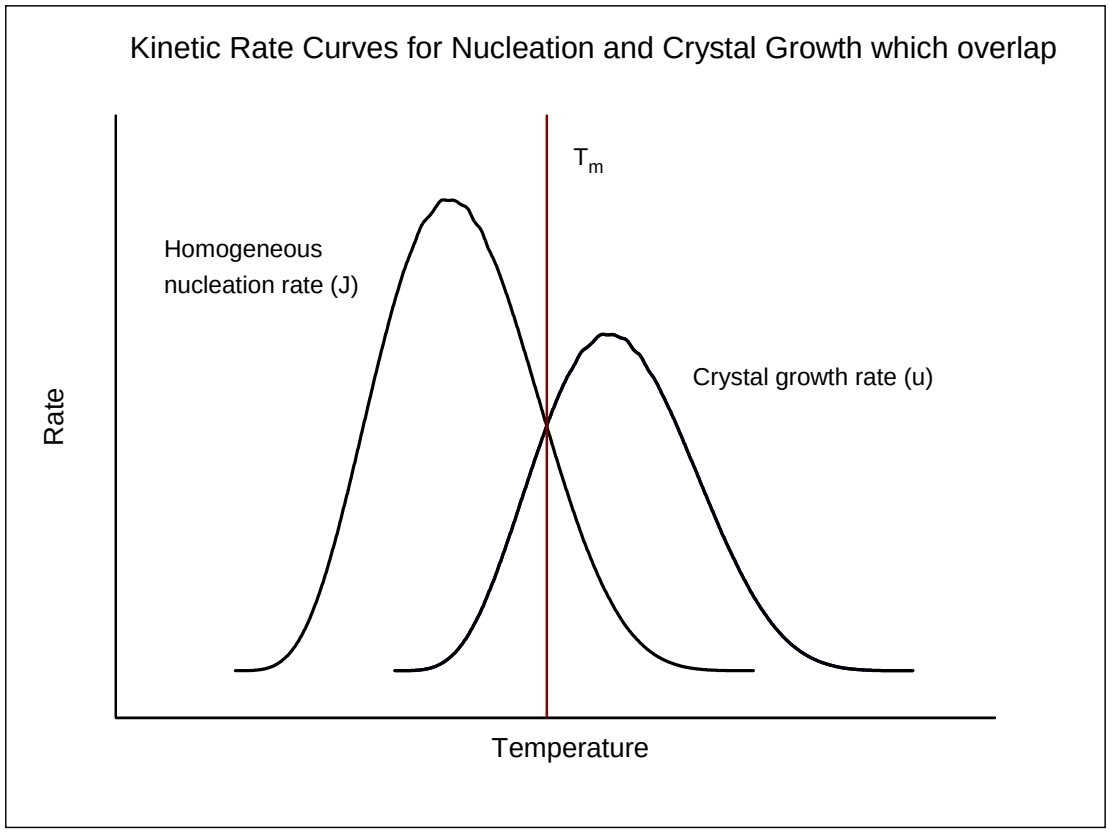

Figure 1.2a
Kinetic rate curves for homogeneous nucleation and crystal growth where both processes are fast at a temperature T_m

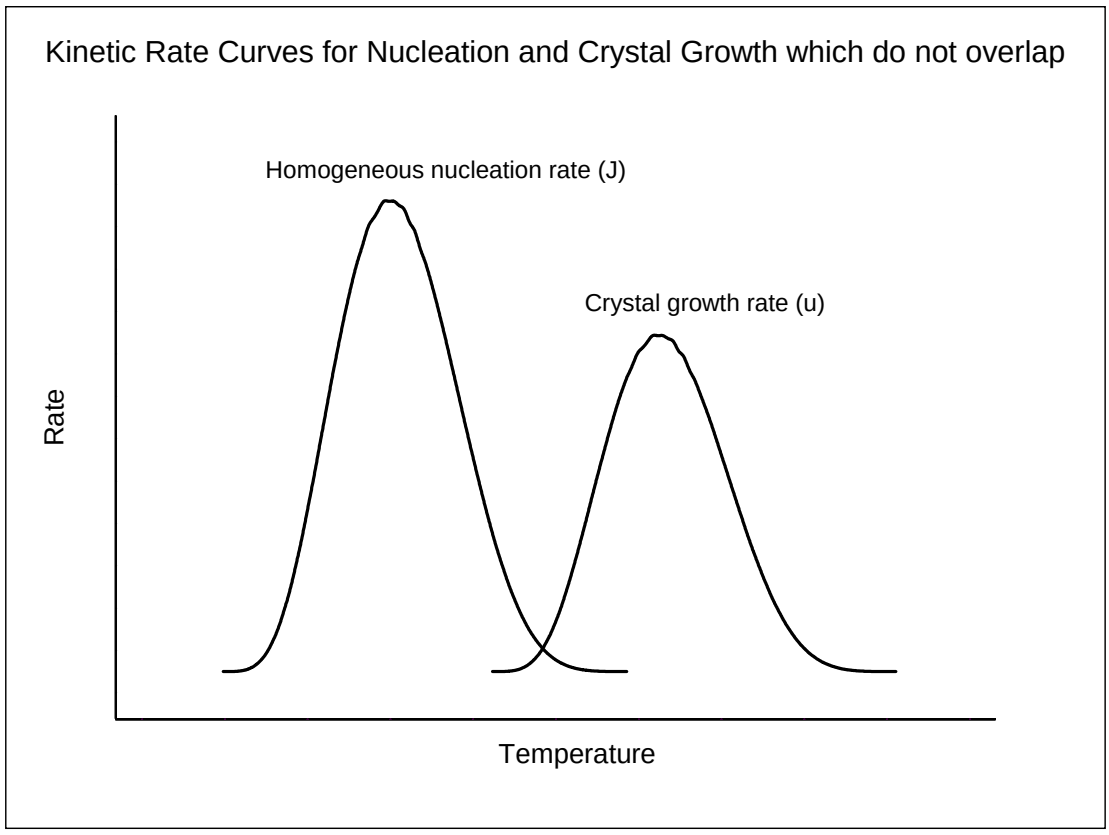

Figure 1.2b
Kinetic rate curves for homogeneous nucleation and crystal growth where the processes are not both fast at any one temperature

2 Experimental

The freezing data for nitric acid aerosols with compositions between 0.25 and 0.45 mole fraction were initially reported in Allan Bertram's PhD thesis[20]. Enough detail is described herein to assist the reader in understanding the results of the analysis presented in this thesis. In the first section of this chapter, general considerations and apparatus for the measurements described in this thesis will be discussed. In subsequent sections, methods specific to the individual systems will be discussed in detail.

2.1 General Experimental Apparatus:

2.1.1 Cryogenic Flow Tube

Acid aerosols were observed in a cryogenic flow tube as depicted in figure 2.1. The flow tube has an inner diameter of 3.5 inches, and is composed of three copper sections. The first two sections are nine inches long, while the final observation section has a length of 23 inches. Each section is independently cooled by liquid nitrogen flowing through 1/4 inch copper tubing, which is soldered to the outside of the flowtube. Thermal isolation between sections is achieved by placing thin walled stainless steel bellows between them. The entire flow tube is then isolated from the laboratory environment by means of a six-inch square stainless steel vacuum jacket. Gas, and/or aerosols are injected into the inlet at the top of the flow tube.

The temperature of the material is determined using ten type T (copper/ constantan) thermocouples located at various positions along the tube. Temperatures are measured throughout the experiment. For the flow conditions used in all experiments, the temperature at the wall of the flow tube does not vary by more than 1.6 K from that along the centre axis of the tube. This is the uncertainty in the temperature measurement itself.

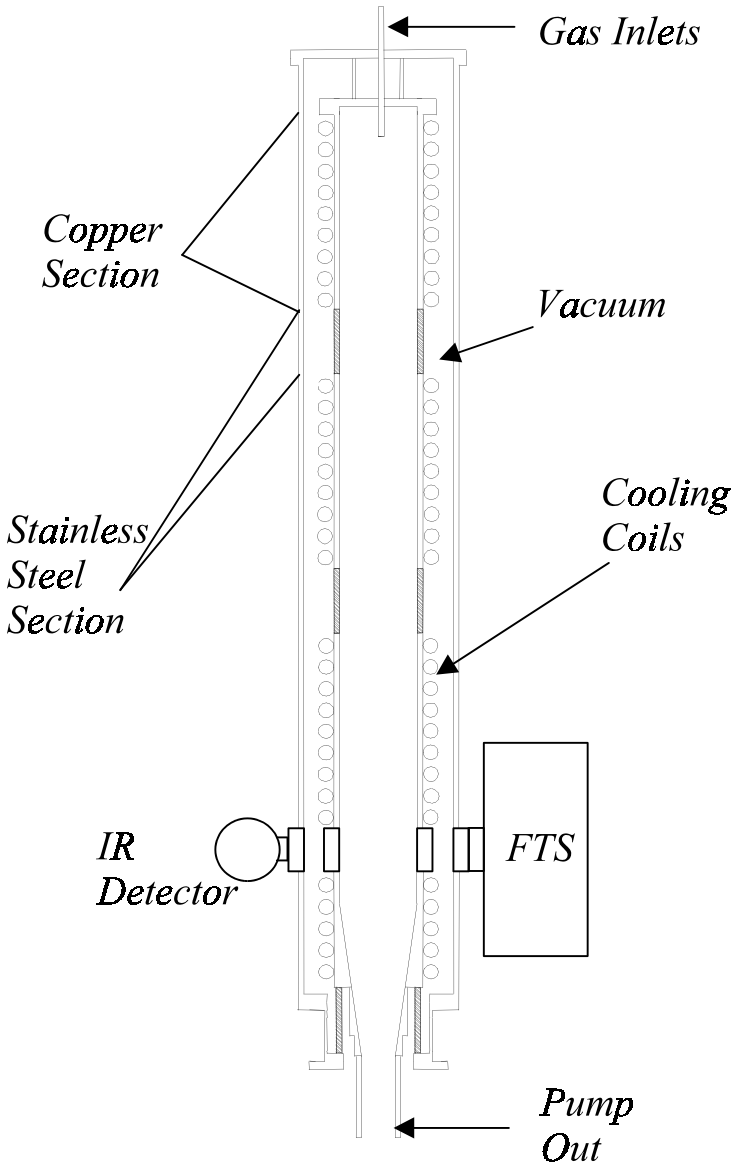

Figure 2.1
Cryogenic flow tube used in cloud nucleation experiments

Temperature gradients along the axis of the flow tube were observed in experiments where higher flow rates were used. In these cases, the coldest temperature observed was reported.

2.1.2 IR Spectroscopy of liquids and solids

Observation of the aerosols is accomplished using FTIR extinction spectroscopy in the final section of the flow tube through ZnS windows. Spectra were recorded using a Mattson 6021 tabletop Fourier transform spectrometer and external MCT detector, operating at 4 cm^{-1} resolution. By observing positions and relative intensities of the bands present in the aerosol spectrum, it is possible to determine the size as well as phase of the aerosols being observed.

When radiation encounters small particles (the particle radius is of the same order of magnitude as the wavelength of the light), extinction occurs due to both scattering and absorption. Mie theory predicts the scattering and absorption of light if both real and imaginary refractive indices are available. Although Mie theory was introduced early this century, it was not until the advent of the digital computer that it became possible for it to be used for modelling laboratory measurements[21].

We assume that aerosols observed in the flow tube have a log-normal size distribution (equation 2.1)[18,22], where r_g is the geometric mean radius, and σ is the standard deviation, which measures the amount of spread in the distribution. This allows forward calculations of spectra for any valid set of lognormal parameters. We can then use a simple fitting algorithm based on the simplex method given in *Numerical Recipes in Fortran*[23] to obtain the size parameters (r_g and σ) as well as number densities for aerosols observed in the flowtube.

$$f(r) = \frac{1}{\sqrt{2\pi r}\,\ln(\sigma)}\, e^{\left[\frac{(\ln r - \ln r_g)^2}{2(\ln\sigma)^2}\right]} \qquad (2.1)$$

There are difficulties with this method, however, as multiple size distributions may give equally good fits. The generation of contour plots of the spectral fit parameter, c^2 versus r_g and σ, can be somewhat enlightening for spectra where this is the case. If the contour shows the best fit lying along a valley in the contour, then no size distribution can be determined for the aerosol, although a meaningful range of size parameters may be determined.

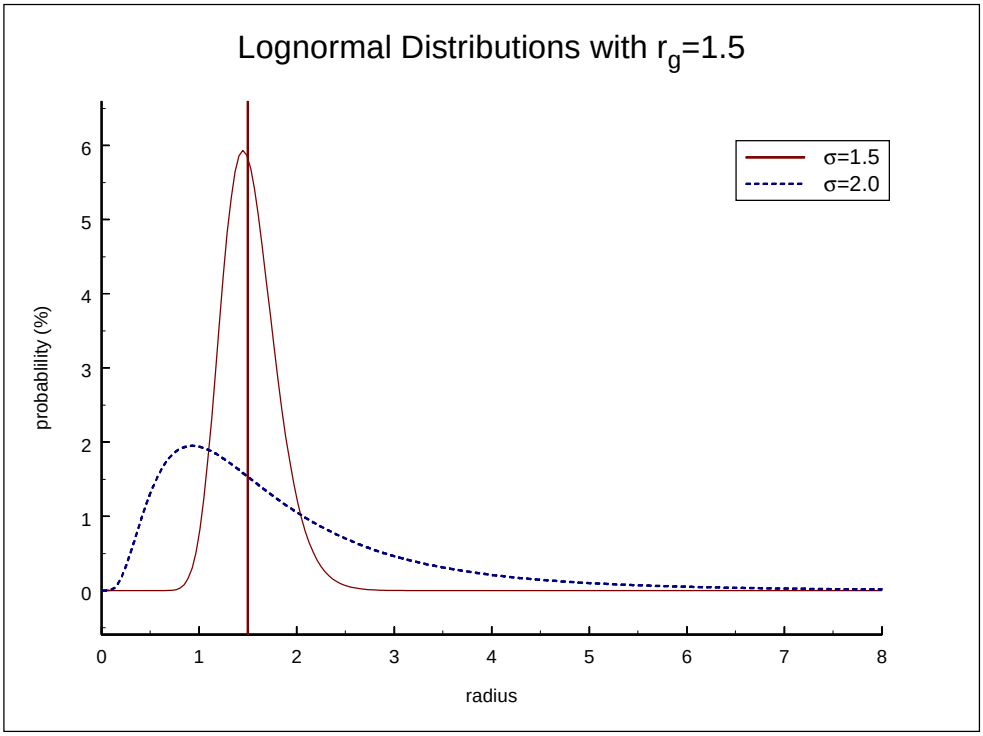

Figure 2.2
Lognormal distributions with geometric mean radius of 1.5 μm and deviations of 1.5 and 2.0

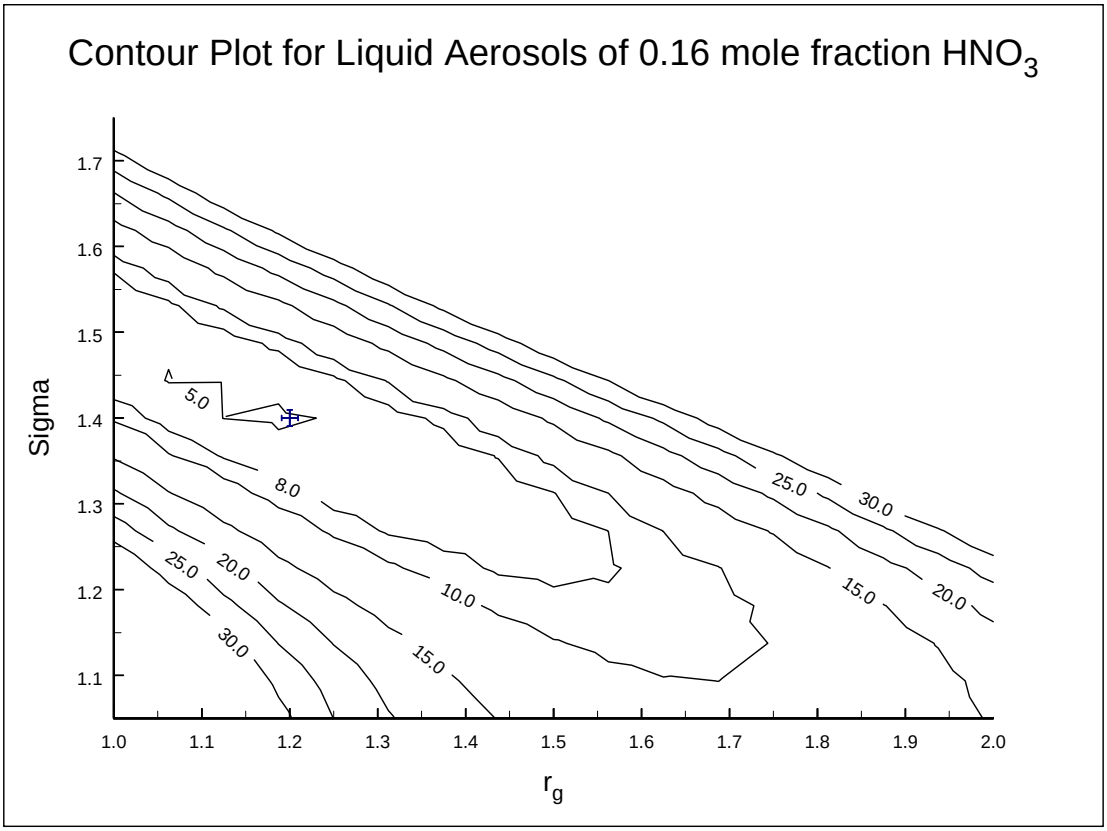

Figure 2.3
Contour plot for liquid HNO_3/H_2O aerosols with a composition of 0.16 mole fraction HNO_3.
Optical constants taken from Biermann et al.[39]
The cross represents the result from the minimization program.

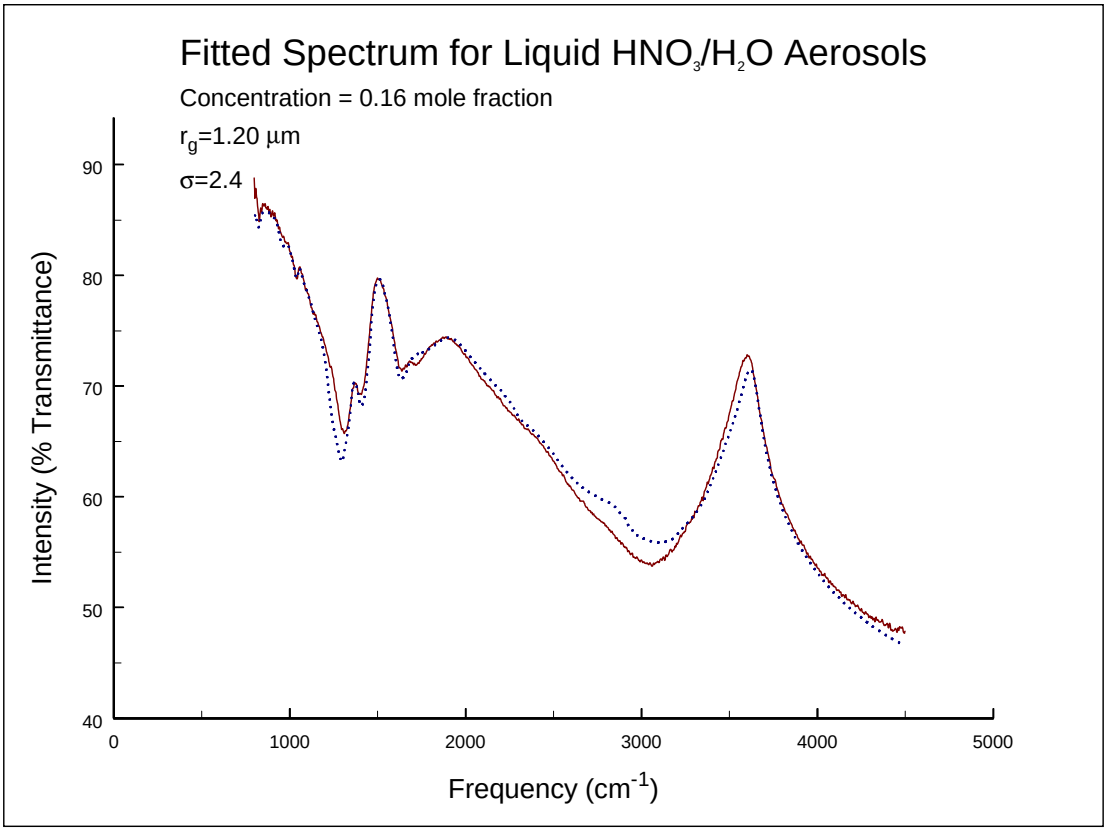

Figure 2.4
Fitted spectrum (dotted line) for 0.16 mole fraction HNO_3/H_2O aerosols.

As stated earlier, Mie theory is only accurate for spherical particles. However, the smaller the particles, the more accurate it is to treat non-spherical particles as spherical. Non-spherical ice crystals were modelled using an approximation in which the aerosol particle is treated as a matrix of dipoles whose properties are determined by the refractive indices for the substance[24]. An electromagnetic wave is propagated through this matrix of dipoles and its trajectory and amplitude determined. This calculation is done for a large number of orientations for the particle shape being studied, and cross sections for extinction are determined. Although this model works well for any shape of particle, it is very computationally expensive, and extensive use of this model for fitting spectra is not feasable. Figure 2.5 shows the difference between spherical ice particles and hexagonal rod with 10:1 length:width ratio, calculated using the dipole approximation.

It has also been reported that when aerosols have a distribution of sizes, shape effects are also removed from the spectrum[25,26]. This is due to the presence of small particles which, as demonstrated by figure 2.5, exhibit scattering which is more similar to spherical particles. This is particularly true for broad distributions which tend to have high frequencies for small particles.

Because crystalline aerosols form from liquid droplets, which due to surface tension should be approximately spherical, it seems unlikely that they would change shape significantly. As the temperature drops, the viscosity of the liquid also increases, inhibiting significant shape changes in the particles as they freeze. These factors also justify the choice of Mie theory for the modelling of aerosol spectra.

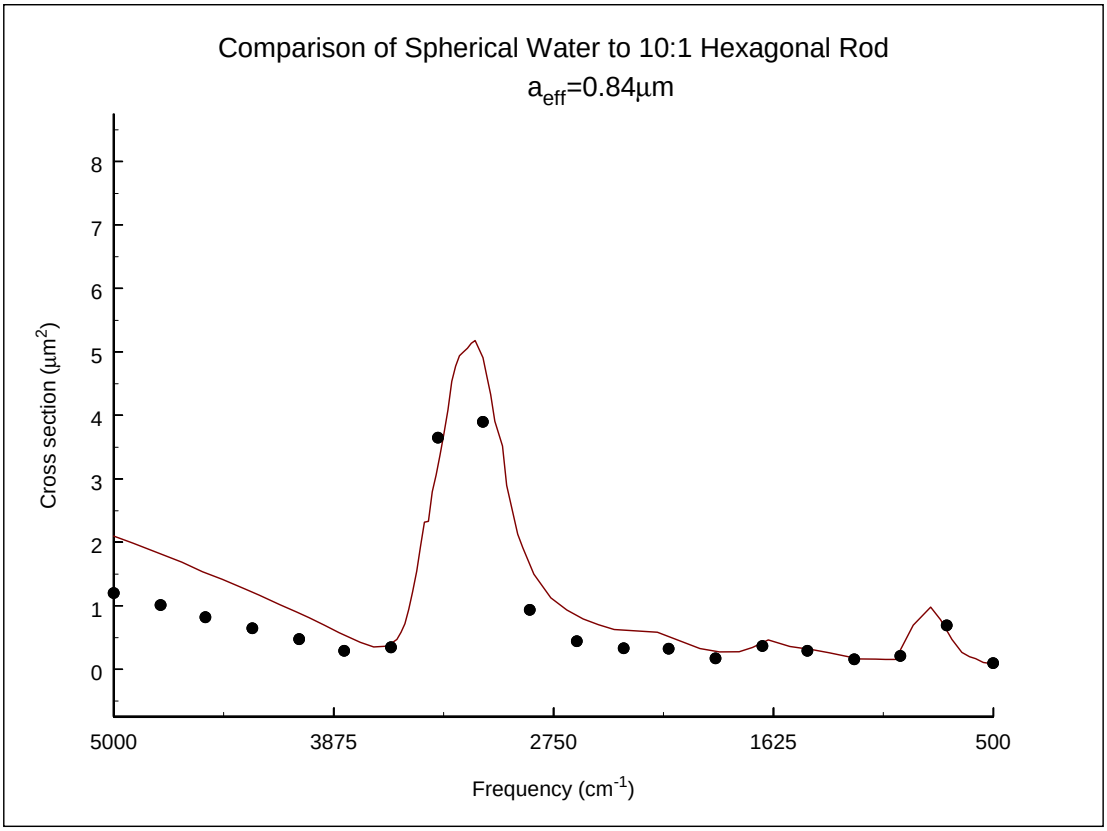

Figure 2.5a
0.8 micron radius spheres (line) and 10:1 hexagonal pillars of equal volume (dots)

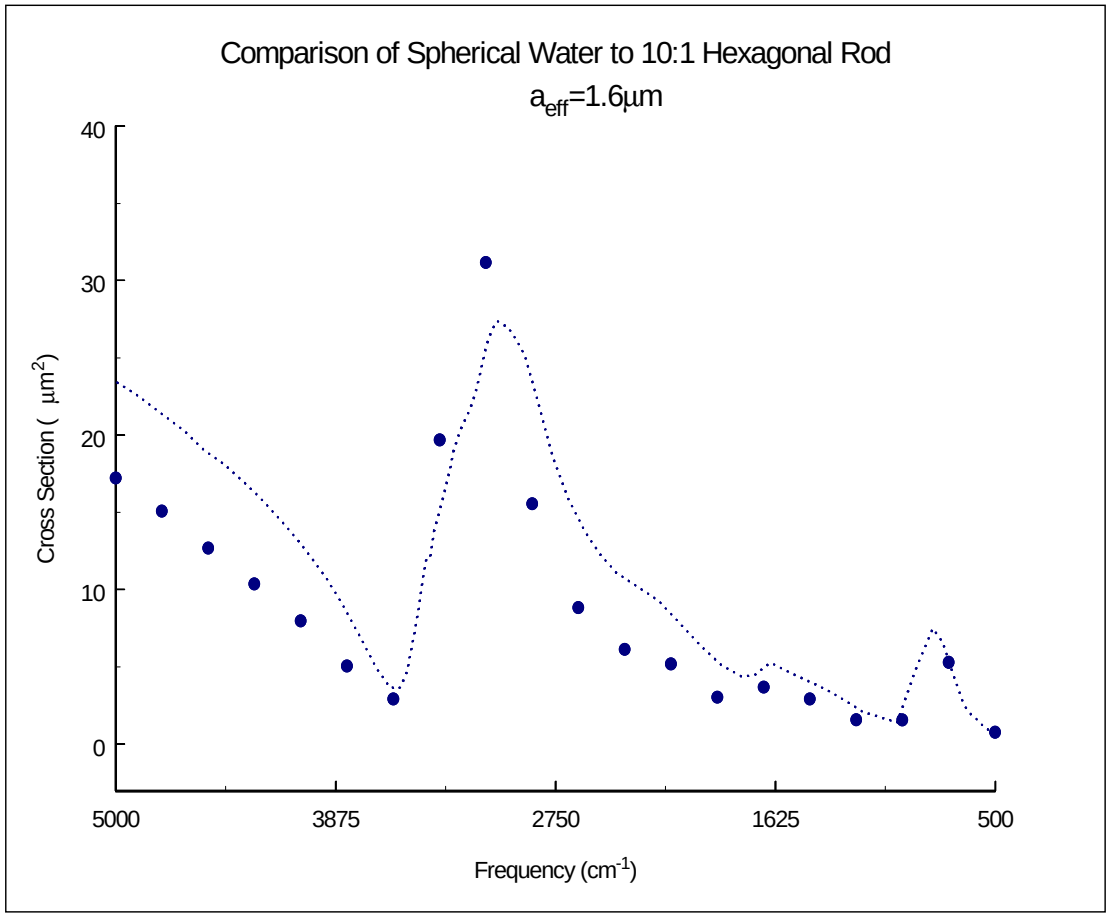

Figure 2.5b
1.6 micron radius spheres (line) and 10:1 hexagonal pillars of equal volume (dots)

2.2 0.25-0.45 Mole Fraction Aerosols

2.2.1 Aerosol Generation

Nitrogen gas was passed over 70% HNO_3 solution and de-ionized water held in separate cylindrical vessels (conditioners). Prior to entry into the top section of the flow tube, dry nitrogen was mixed with the flows that passed through the conditioners. Upon cooling in the top section of the flow tube, water and nitric acid vapour condense to form aerosol droplets with a geometric mean radius of about 0.2 microns. By adjusting the nitrogen flows through each of the conditioners, aerosols with the desired compositions were obtained. The total nitrogen flow was monitored using an OMEGA mass flow meter (model # FMA1818ST), which monitored the gas flow before it was separated into the wet and dry flows.

The total pressure in the flow tube was kept at 250 torr, and the total nitrogen flow rates ranged between 2.5 and 6 standard litres per minute. It was found necessary to increase the flow rate in order to reduce the residence time and hence composition changes due to diffusion of water to the walls. Diffusion is described by the diffusion parameter D[27], given by equation 2.2.

$$D = \frac{1}{3}\lambda\bar{c} \qquad (2.2)$$

λ is the mean free path of water molecules in the nitrogen carrier gas, and $\bar{c}$ is the mean speed of water molecules. The diffusion coefficient has units of m^2s^{-1}. The longer aerosols reside in the flow tube, the more water can diffuse to the cold walls where the vapour pressure is lower than in the region of the aerosol droplet.

2.2.2 Aerosol Freezing Measurements

Once liquid aerosols were formed at approximately 190 K, they entered the second section of the flow tube, which was also kept at approximately 190 K. The temperature of the final section of the flow tube was varied in order to cause nucleation.

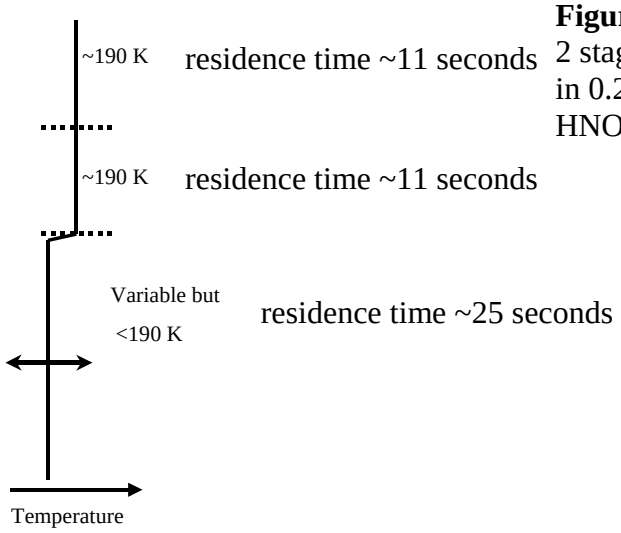

Figure 2.6
2 stage temperature profile used in 0.25-0.45 mole fraction HNO_3 experiments

2.2.3 Composition Determination and Gas Phase Calibration

Concentrations are determined using a Bruker IFS 55, operating at 0.5 cm^{-1} resolution, which samples the gas resulting from the vapourization of aerosols as they exit the flow tube. The aerosols are evapourated, and the resulting vapour spectrum is measured at approximately 294 K. A sample spectrum is plotted in figure 2.7. The areas of the 1889 cm^{-1} and 1990 cm^{-1} water peaks were used with an appropriate calibration (described below) in order to determine the vapour pressure of water in the cell. The nitrate band located at 760 cm^{-1} was was used to determine the vapour pressure of nitric acid. The ratio of the vapour pressures yields the concentration of nitric acid within the aerosols before they were vapourized.

Calibration was accomplished by slowly flowing nitrogen gas over nitric acid solutions of known concentration. Using activity data for nitric acid and water vapour over a solution of known concentration[28], the vapour pressures of nitric acid and water in the gas cell were determined. Infrared spectra were recorded and the peaks corresponding to water and nitric acid (listed above) were integrated and their areas recorded versus partial pressure of the appropriate gas within the cell. The resulting calibration curves are shown in figures 2.8 and 2.9. Using these curves, the relative concentrations of nitric acid and water, and hence, the mole fraction of nitric acid in the aerosols was determined.

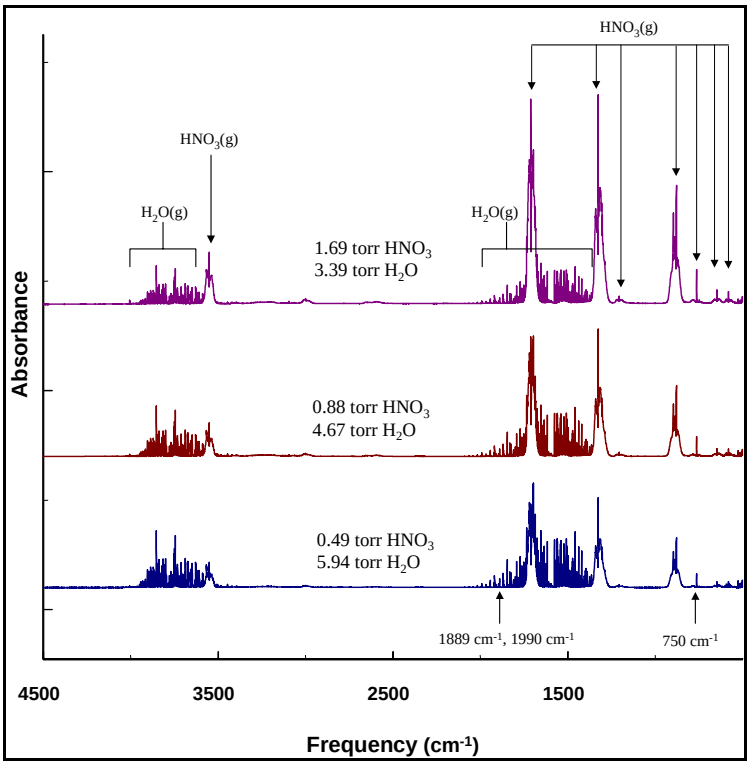

Figure 2.7
Sample spectra used in the gas phase calibration for 0.25-0.45 mole fraction HNO_3 experiments

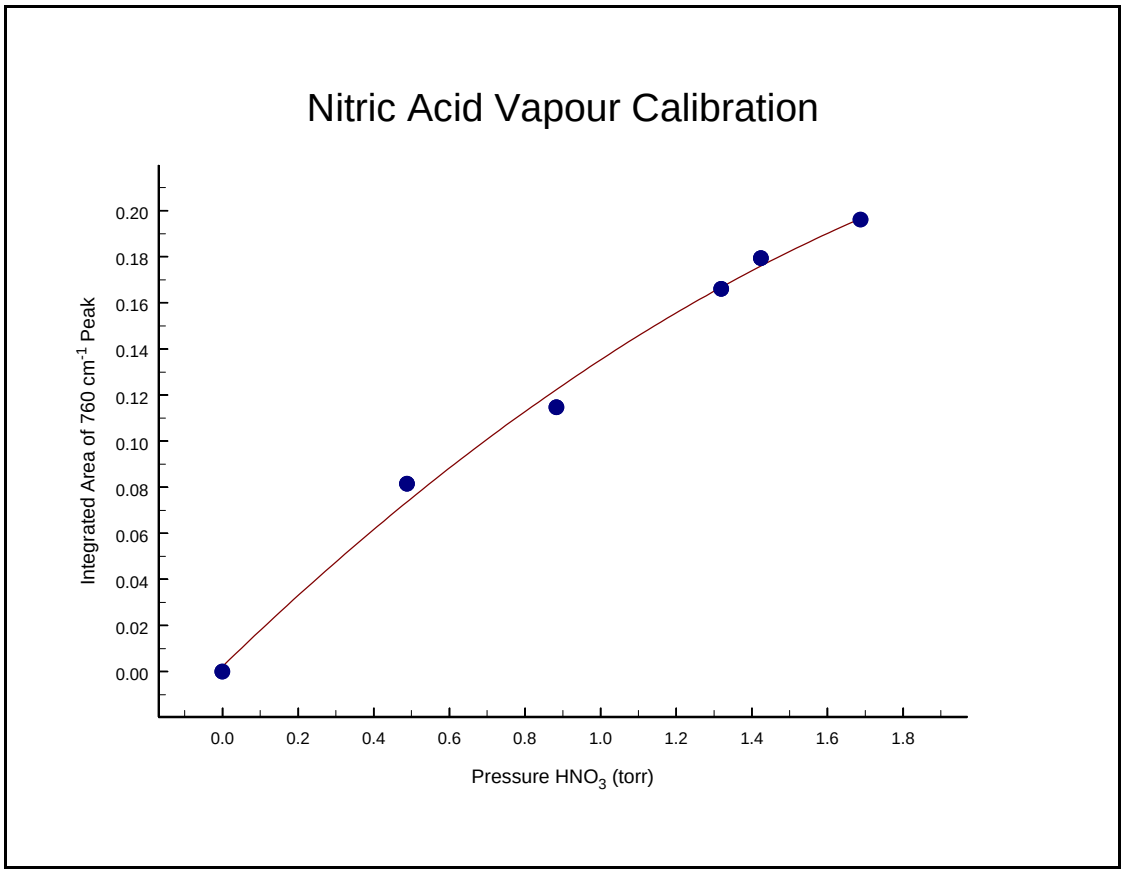

Figure 2.8
Nitric acid calibration for 760 cm^{-1} band at 250 torr

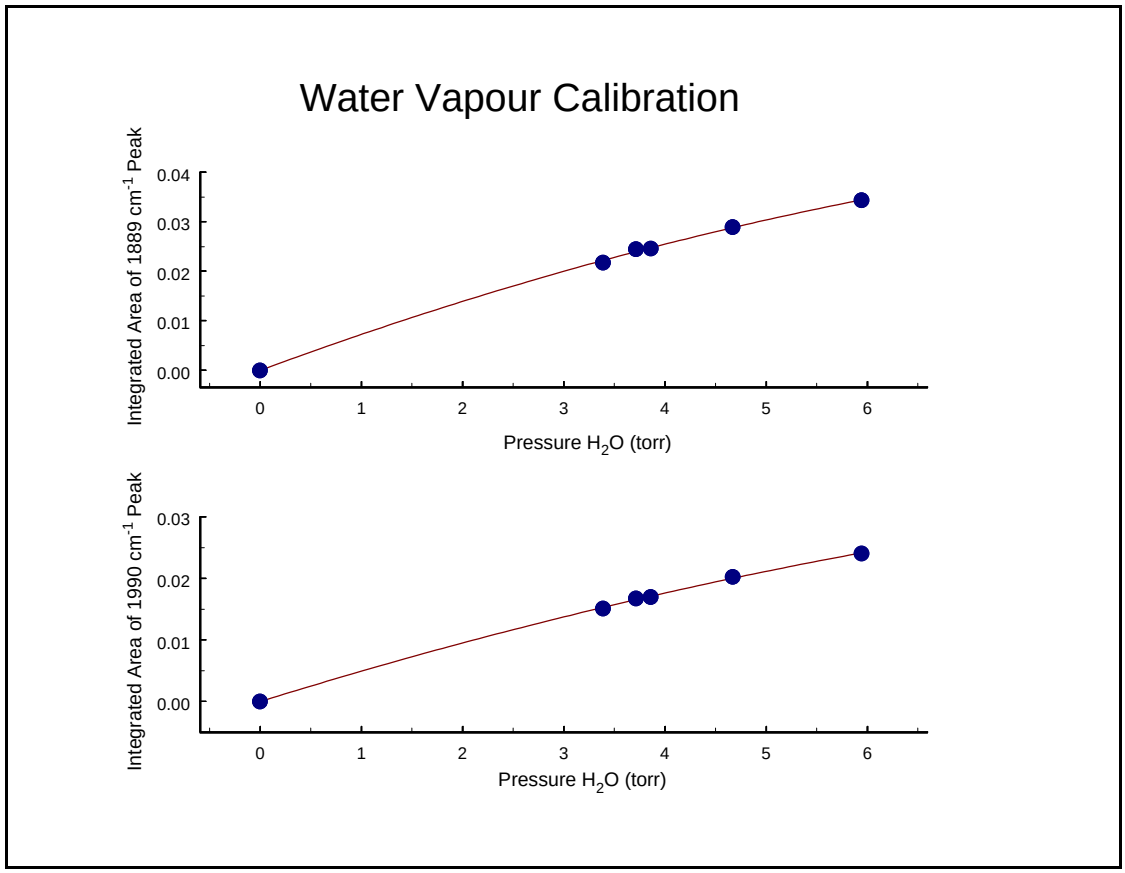

Figure 2.9
Water calibration for 1889 cm^{-1} and 1990 cm^{-1} peaks at 250 torr

2.3 0-0.25 Mole Fraction Aerosols

2.3.1 Aerosol Generation

Because of the high vapour pressure of water over dilute nitric acid solutions, the method of aerosol generation described in section 2.2.1 could not be used for these aerosols. When nitric acid and water vapour were introduced into the flow tube under the conditions described previously, water vapour would condense onto the walls of the flow tube as ice, rather than homogeneously condensing to form aerosol droplets. This problem was overcome by increasing the pressure from 250 to 750 torr, as well as by increasing the flow rate to 5 standard litres per minute. Also, aerosols were generated using a DeVilbis utralneb 99 ultrasonic nebulizer and introduced as liquid droplets into the top of the flow tube. The size distribution of aerosols generated by this device was found to have a geometric mean radius ranging from 0.7 to 2 microns. These size distributions tend to be more realistic models for cirrus cloud particles, which are believed to contain more dilute concentrations of nitric acid[29].

Nitrogen gas was passed through the nebulizer chamber, collecting liquid nitric acid aerosols. This flow was mixed with dry nitrogen in order to reduce the number density of aerosols to the amount desired, and the resulting flow was injected into the top section of the flow tube where it was cooled to approximately 240 K.

2.3.2 Aerosol Freezing Measurements

The temperature in the middle section of the flow tube was varied in order to study the nucleation temperature. Aerosols were annealed in the final section at a temperature that varied from 10 to 30 K warmer than the temperature of the middle section. By raising the temperature in the third section, we create more favourable conditions for crystal growth in the sample after nucleation occurs in the second middle section. An infrared spectrum was recorded in the final section of the flow tube using a

Mattson 6021 FTIR spectrometer operating at 4 cm^{-1} resolution. Spectra were recorded as a function of temperature. The changes observed in these spectra as a the temperature changes will be discussed in the next chapter.

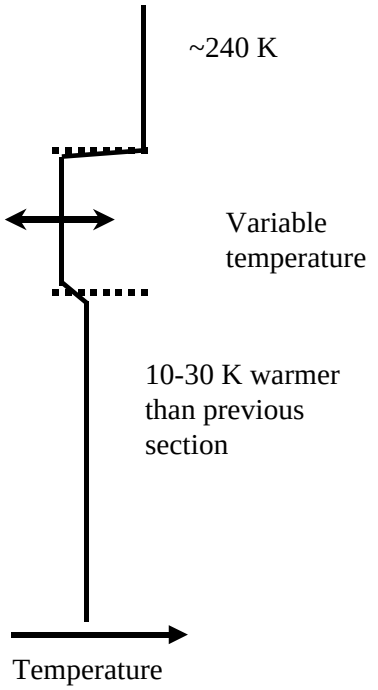

Figure 2.10
3 stage temperature profile used in 0-0.25 mole fraction HNO_3 experiments

2.3.3 Gas Phase Calibration

Because diffusion is much slower at larger pressures[27], the method of generating the calibration curve described in section 2.2.3 could not be used for calibration at 750 torr. As the pressure increases, it becomes more difficult to saturate the nitrogen carrier gas with vapour, which is required condition for the activity model used.

Water calibration was accomplished using an OMEGA dew point hygrometer (model # RHB-1A). Nitrogen carrier gas was flowed over deionized water, and then mixed with dry nitrogen to produce the desired vapour pressure of water. This mixture of

nitrogen and water vapour is passed over a mirror inside of the dewpoint sensor. A laser determines the temperature at which a film forms on the mirror by cooling or heating the mirror until its optical properties are changed by condensation. This is detected using laser diode. The vapour pressure that was obtained from the CRC handbook[30] based on the measured dewpoint. Water vapour peaks at 1575 cm^{-1} and 1845 cm^{-1} were integrated, and their areas used to prepare a calibration curve.

For HNO_3 calibration, nitric acid solution was placed in the cell allowed to sit until equilibrium was established between the gas and liquid phases. IR spectra were then taken and the area of the 900 cm^{-1} peak corresponding to nitric acid vapour was determined. The peak at 900 cm^{-1} was used because it is does not overlap with the gas-phase water spectrum, and has sufficient intensity. The water calibration curve (described above) was used to determine the vapour pressure of water above this solution. The activity model (referenced in 2.2.3)[28] was then used to determine the concentration of the solution. Once the concentration of the solution had been determined, the pressure of nitric acid vapour was determined using the same activity model. This procedure was repeated for various concentrations and the calibration curves shown in figure 2.11 and 2.12 were produced.

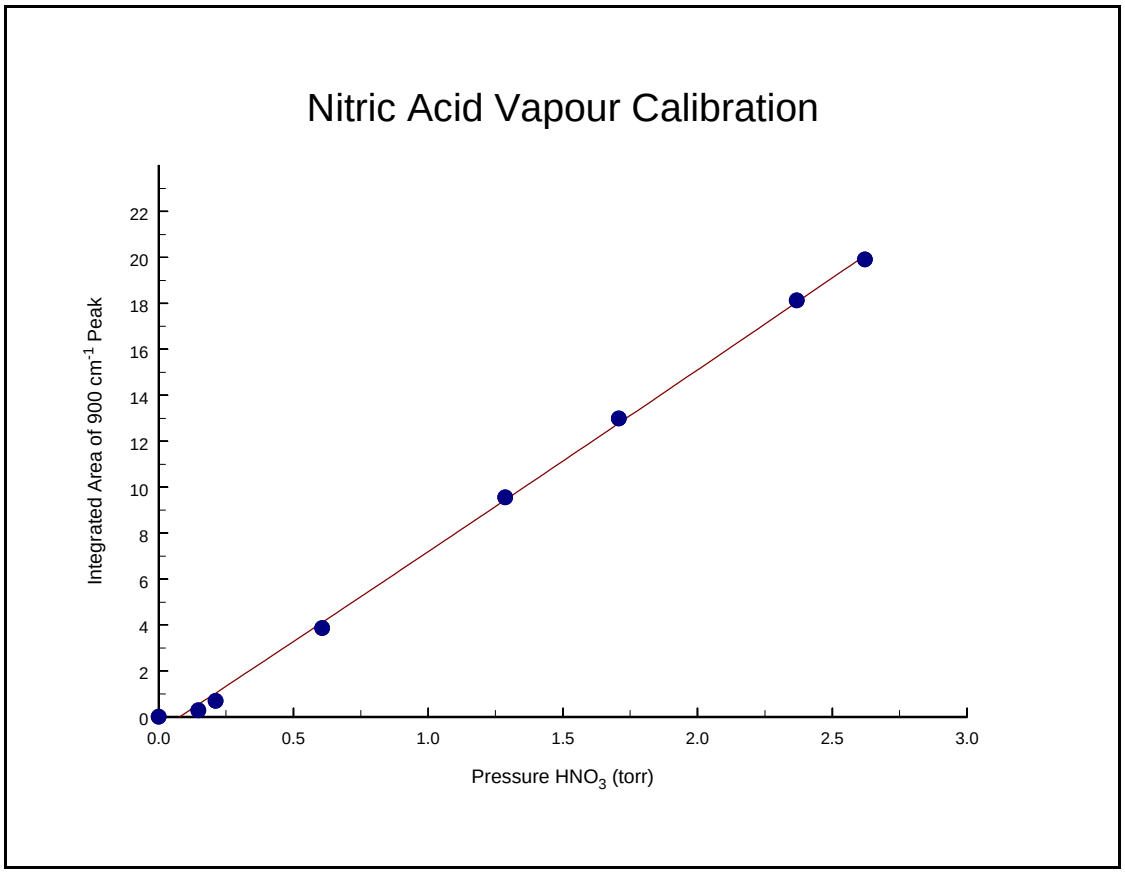

Figure 2.11
Nitric Acid Calibration using 900 cm^{-1} band at 760 torr

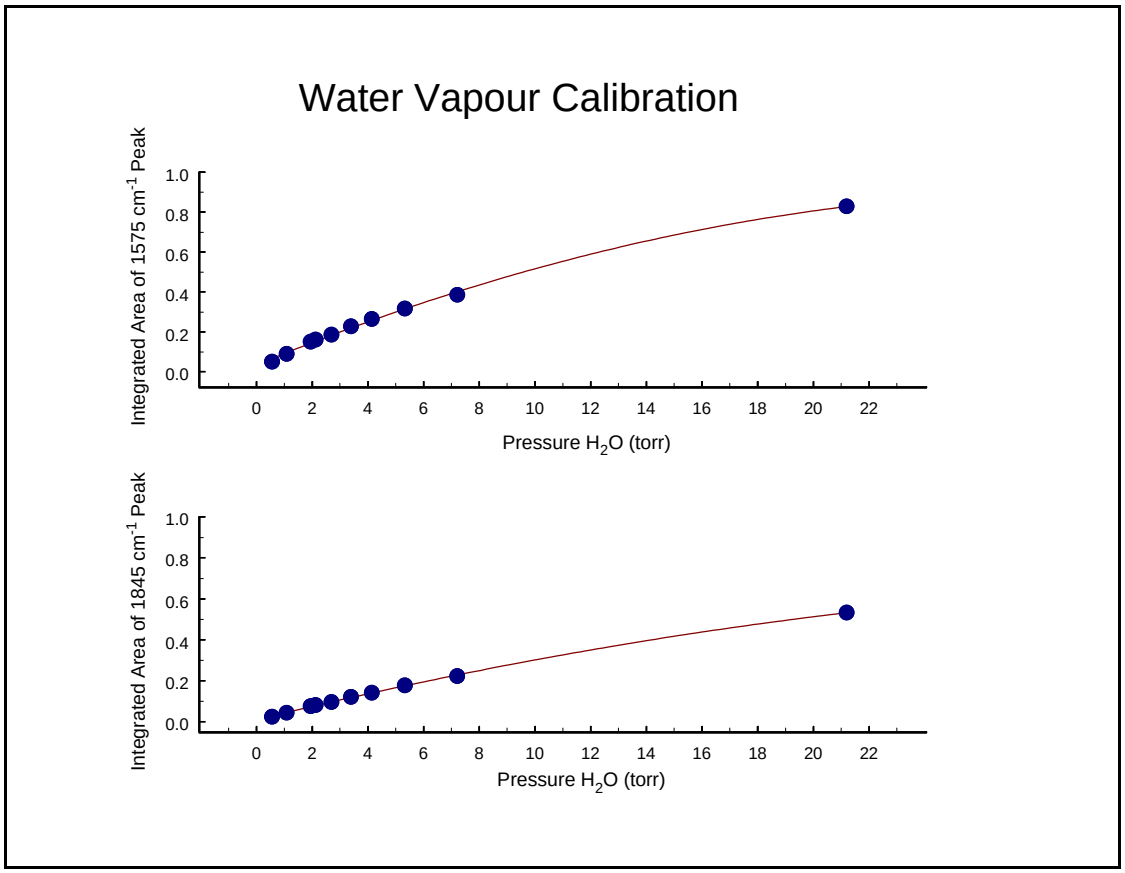

Figure 2.12
Water calibration for 1575 cm^{-1} and 1845 cm^{-1} peaks at 760 torr

3 Results and Discussion

As with the previous chapter, this chapter is divided into two parts. The first part of this chapter will describe the analysis of the 0.25-0.45 mole fraction experiments treated previously in Allan Bertram's Ph.D. thesis[20]. This data was later examined, as described in this thesis, using a more comprehensive analysis scheme. In the second part of this chapter, the results of the investigation of 0-0.25 mole fraction HNO_3 aerosols will be discussed. And finally, the atmospheric implications of these data will be discussed briefly.

3.1 0.25-0.45 Mole Fraction Aerosols.

The freezing behaviour of nitric acid/water particles varies as a function of concentration. Due to the limited residence time of aerosols in the flow tube, it is not always possible to acheive complete crystallization. Thus it was the aim of this work to identify the temperature at which crystallization first appears, and to determine the species of the crystal formed (either nitric acid hydrate or ice) , when crystallization is observed. When possible, the evolution of the particle composition during freezing will also be discussed. The proceedure by which we may determine these properties is the linear least squares method. Using this technique, spectra are assumed to be composed of a certain number of spectra which form a basis set.

3.2 The Linear Least Squares Method

If we consider a spectrum consisting of points S_n, where n is the number of points in the spectrum, and a basis set consisting of three spectra, A_n,B_n,and C_n, then S is composed of only A, B and C in some linear combination. This gives us n equations of the form $S_n=aA_n+bB_n+cC_n$, where a, b, and c are some non-negative, real number

coefficients. As long as there are at least three spectral points, we should be able to solve for the coefficients and determine the relative weighing of each of the basis spectra in S. There are several issues that must be attended to with this method of data analysis however, in order to ensure the validity of the results obtained. These will be discussed below.

3.2.1 Choice of Basis Set for HNO_3/H_2O Spectra

There are only four known species which could crystalise out of HNO_3/H_2O aerosols. These crystals are Nitric Acid Monohydrate (NAM), Nitric Acid Dihydrate (NAD), Nitric Acid Trihydrate (NAT) and water ice (referred to simply as ice). In this concentration region of the phase diagram however (see figure 3.1), the only phases which could be present are NAM, NAD, NAT, and liquid. Water is not thermodynamically stable under these conditions.

Barton et al.[31] have shown that NAM does not crystalise in submicron sized aerosols, even during time scales on the order of minutes (The total residence time in the flow tube was less than 1 minute in our experiments), and hence NAM crystals should not be observed in our experiments. Our observations, as will be discussed below, support this assumption. Hence, the basis set selected consisted of NAD, NAT and liquid spectra. The NAD and NAT spectra were calculated using MIE theory and optical constants obtained from Niedziela et al.[32], and the liquid spectra were measured just before the first appearance of solid in each sample. This was done by comparing successive spectra from coldest to warmest, and taking the first spectrum for which no change was detected when compared to the next warmest measurement.

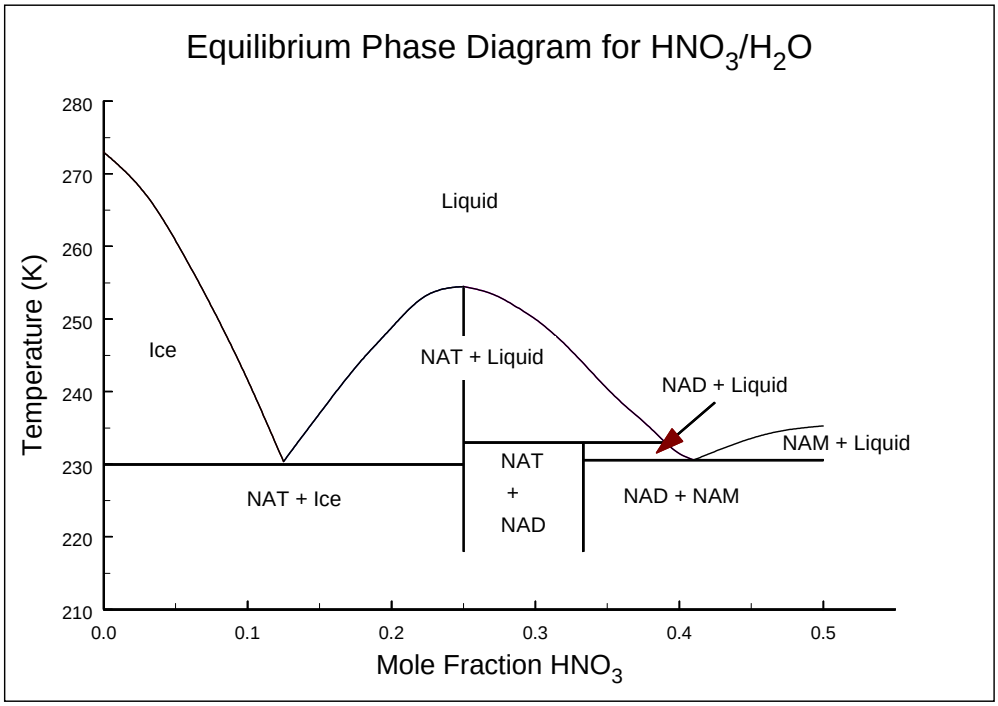

Figure 3.1
Equilibrium phase diagram for HNO_3/H_2O

3.2.2 Particle Size Effects

The scattering component of the IR extinction for small particles is size dependent. Not only the intensity, but also the shape of the spectrum changes as a function of particle size. This size effect is demonstrated in figure 3.2 (next page). This figure displays Mie theory calculations based on the optical constants of Niedziela et al.[32]. Both spectra have a standard deviation (σ) of 1.6, which is representative of the aerosol particles observed in the flow tube. The sizes shown are 0.2 μm and 0.02 μm. 0.2 μm radius is representative of geometric mean radius observed in the experiments, and 0.02 μm is representative of crystals in partially frozen aerosols. The spectra were normalized at the intense peak near 1450 cm^{-1}. If we examine the part of the spectrum between 1000 and 2000 cm^{-1}, we see there is only a 4% difference between the spectra shown. These spectra represent a difference in volume of 1000 times, which also represents a difference of 1000 in spectral intensity. If the experimental signal to noise is 100, the smaller particles would not be detectable, and in this case the error involved in this approximation less than 4%. Because all of the aerosol samples studied had similar size distributions, this estimated error is not expected to differ significantly between experiments.

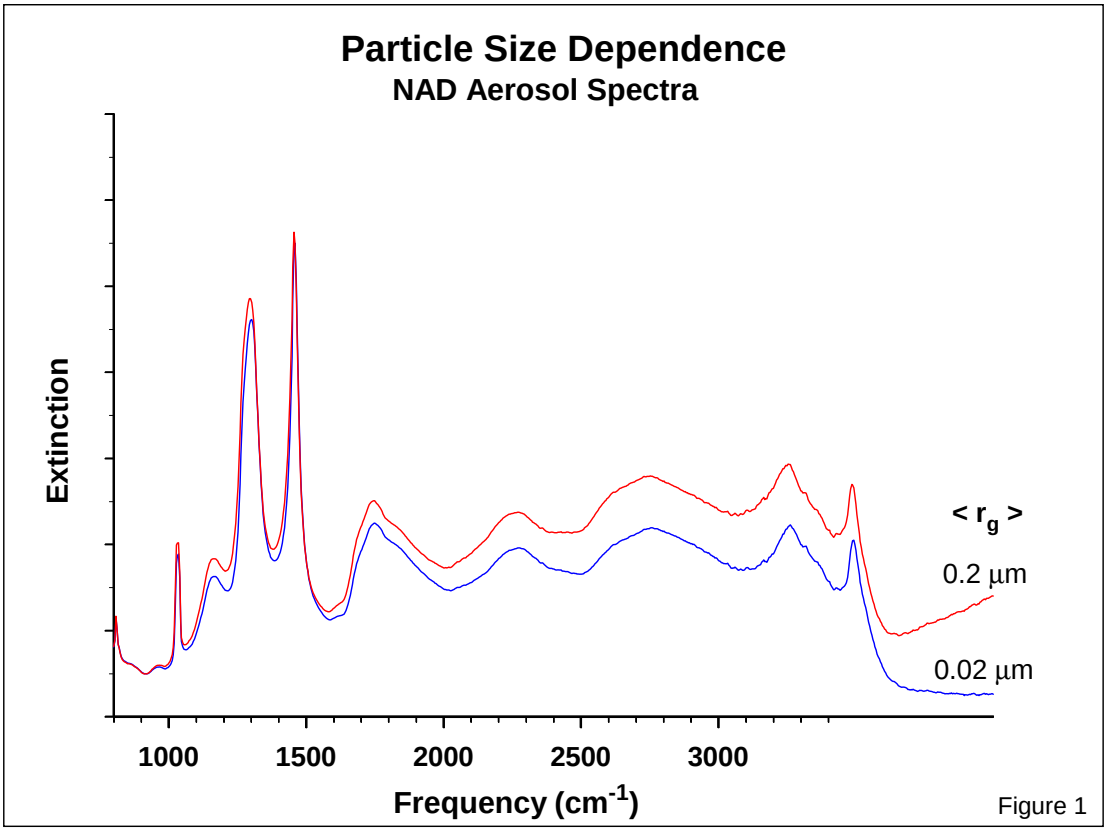

Figure 3.2
Mie theory calculations showing the effects of scattering. Spectra are normalized at 1460 cm^{-1}

3.2.3 Effects of Variable Liquid Composition

As a liquid aerosol particle freezes, the composition of the liquid will change if it is not the same as the composition of the solid phase which is precipitating. Aerosols with mole fractions greater than 0.25 would become less concentrated as NAD or NAT precipitate. Liquid spectra with mole fractions of HNO_3 between 0.24 and 0.46 are shown in figure 3.3. The spectra were recorded just before freezing, and were normalized to intensity of the peak near 1300 cm^{-1} These concentrations bracket those covered by this analysis. The liquid spectra for $0.46<x HNO_3<0.33$ are very similar, and the difference in intensity is less than 10%. When the mole fraction decreases below 0.33, the OH band near 3300 cm^{-1} increases significantly in intensity, but the intensity of the nitrate bands between 1000 cm^{-1} and 1500 cm^{-1} remain relatively unchanged. If we consider only the region of the spectrum between 1000 and 2000 cm^{-1}, we find that the maximum difference is 20% (at 1450 cm^{-1}) and the average difference is less than 5% over this range.

Note also that as the aerosol freezes and the composition of the liquid changes, there is also less liquid present to contribute to the spectral intensity. Hence, when a very small portion of the particles are frozen, and the liquid makes up a significant portion of the spectral intensity, the liquid basis spectrum is a very good representation of the liquid present in the spectrum. The less accurate this representation becomes, due to the formation of crystals within the particle, the less contribution this liquid makes to the total intensity of the spectrum. We conclude therefore, that changes in the liquid spectrum cause less than 5% error provided the data analysis is conducted in the region between 1000 and 2000 cm^{-1}.

The arguments presented in this as well as the previous section indicate that the procedure describe herein is valid for the composition range between 0.46 and 0.25 mole fraction HNO_3.

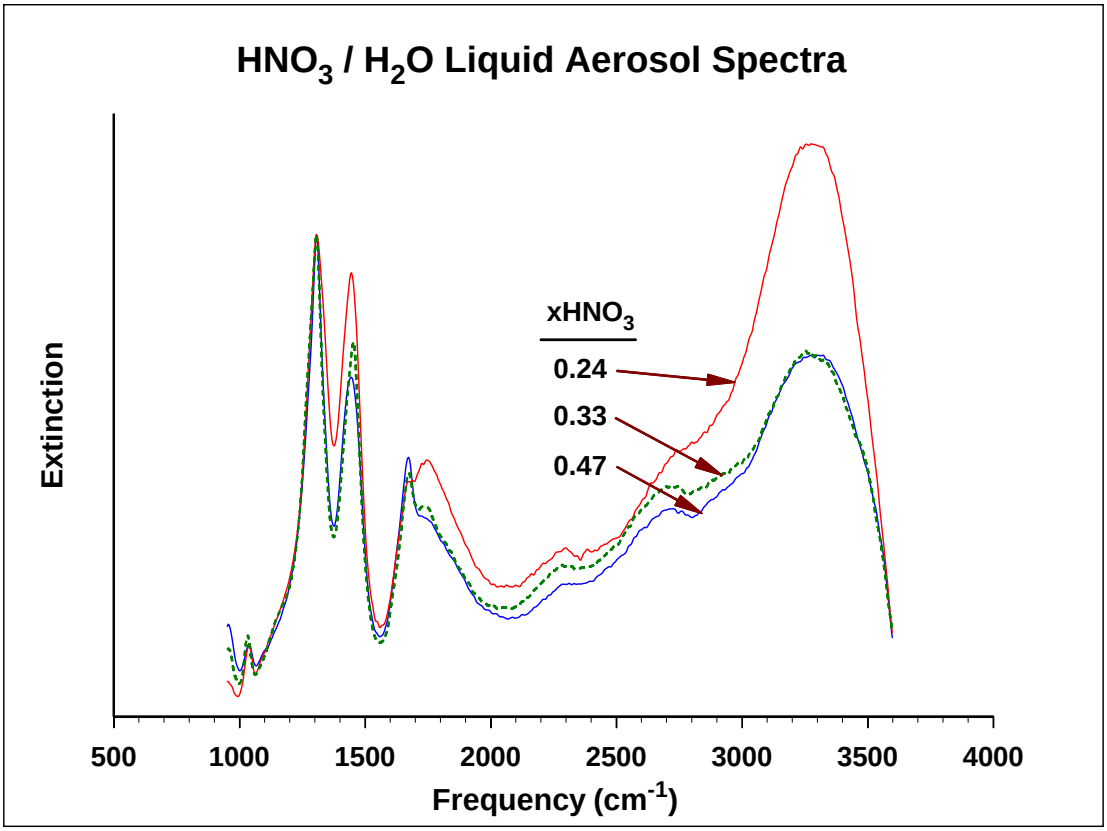

Figure 3.3
Measured spectra of liquid aerosols with radii of approximately 0.2 μm and concentrations as shown

3.3 0.46-0.42 Mole Fraction Aerosols

Spectra of aerosols were recorded at temperatures between 156 K and 186K, using both two and three stage temperature profiles. In both cases, no freezing was observed. Freezing would not be discernable if these aerosols formed amorphous glasses or remain liquid, as the infrared spectra of these two states are very similar. Examining the bulk phase diagram indicates that NAM is formed at this concentration in bulk solutions. However, there is no indication of NAM formation in any of the spectra recorded for this concentration range: even at 156 K, which is more than 80 K colder than the equilibrium freezing temperature. Because no freezing was observed with either temperature profile it is believed that nucleation is the rate limiting process. These observations are in agreement with previous measurements in this temperature range for HNO_3 aerosols[31] as well as thin films[33]. We draw the conclusion, therefore, that nucleation was too slow to be observed in the time frame of these experiments.

3.4 0.33-0.42 Mole Fraction Aerosols

Figure 3.3 shows the evolution of 0.38 mole fraction aerosols with temperature. The spectra appear to undergo a change between 177 and 172 K, which we define as the freezing range. The spectra exhibit very little change at temperatures above and below this range. By applying the linear least squares method described above to this series of spectra, the onset of freezing was determined and the plot in figure 3.4 was constructed.

The basis set used consisted of the liquid spectrum, as well as NAD and NAT spectra calculated from the optical constants of Miller et al.. The size distribution selected for these spectra was r_g=0.2 μm and σ=1.6 μm which matched the size distribution determined for NAD and NAT aerosols generated under similar experimental conditions.

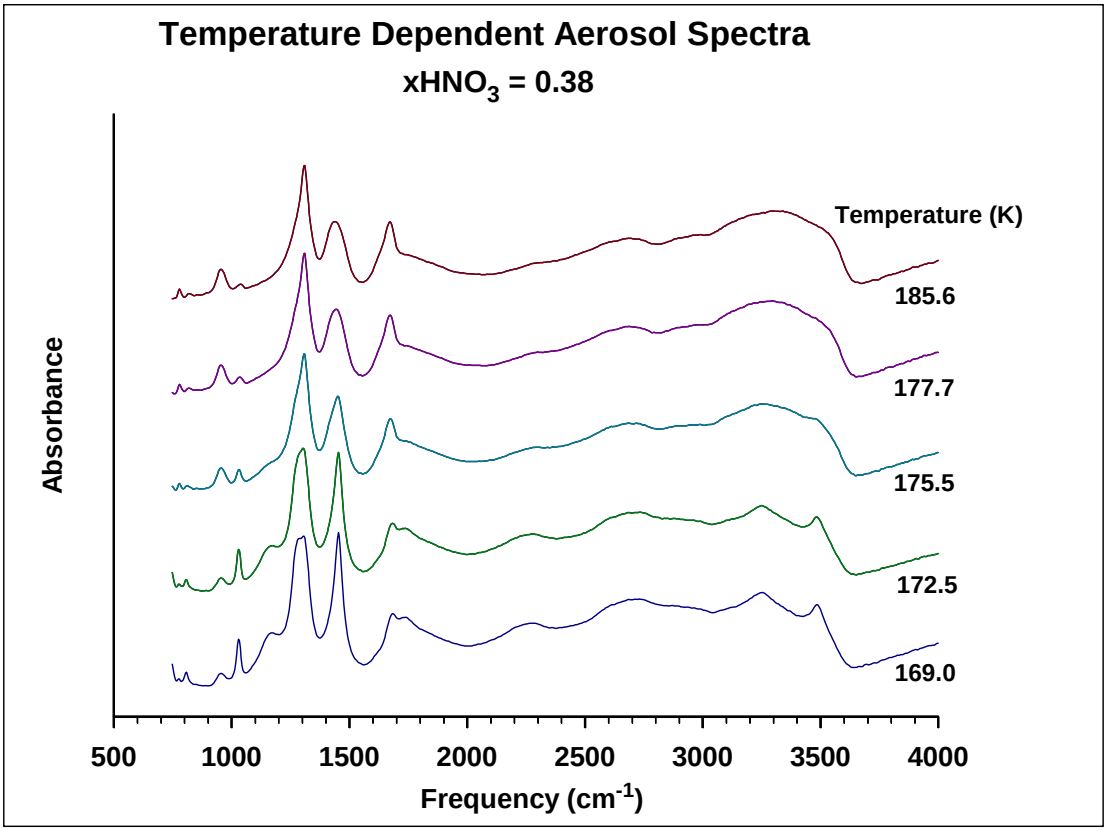

Figure 3.4
Temperature dependence of 0.38 mole fraction HNO_3 aerosol spectra

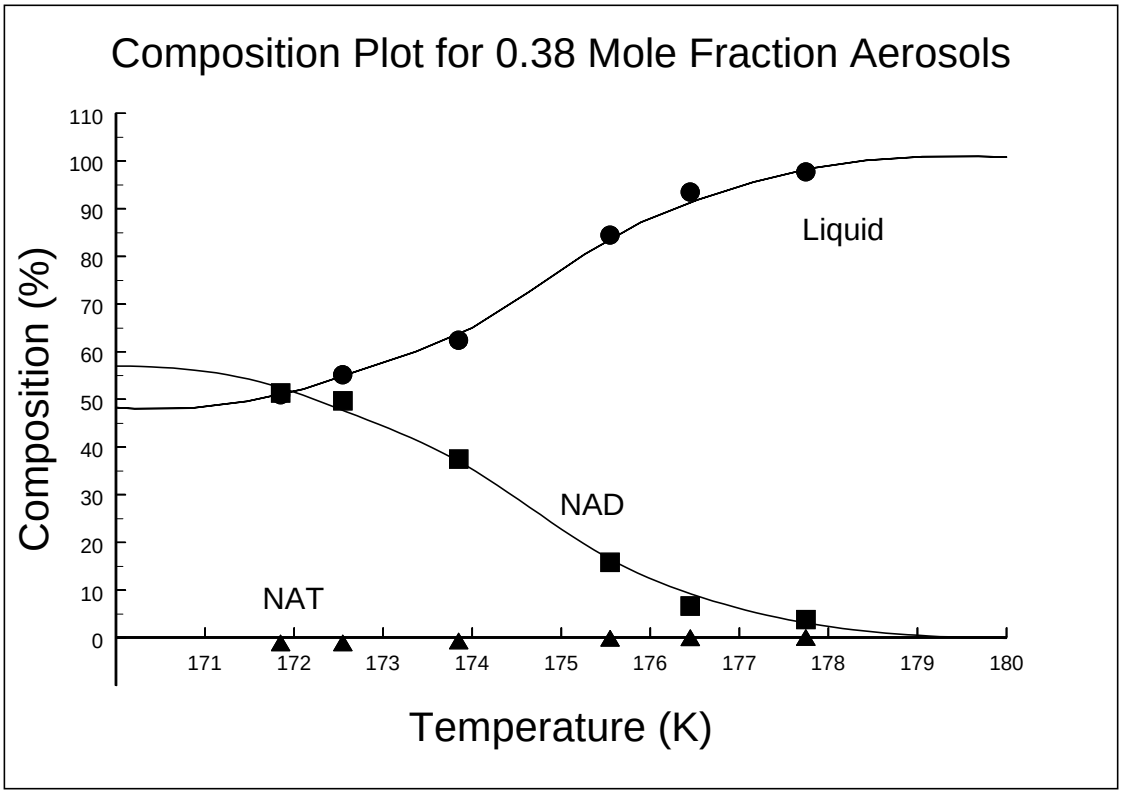

Figure 3.5
Aerosol composition as a function of temperature during freezing process for 0.38 mole fraction HNO_3 aerosols

The coefficients derived from this procedure are given as percent compositions. The onset temperature was taken to be the temperature at which the liquid component drops to 95%. For the 0.38 mole fraction sample shown in figure 3.4, the onset temperature is 177 $\pm$ 1.6 K. 1.6 K represents the uncertainty in the temperature measurement, and the estimated error in the liquid coefficient is 5%, as shown via the error bars on figure 3.8. As indicated in figure 3.4, the solid formed was identified as NAD, and the percentage of NAT stayed below the 5% uncertainty in the coefficients for the entire temperature range studied. This behaviour is characteristic of particles whose compositions are between 0.33 and 0.42 mole fraction HNO_3. Note however, that the NAT coefficients drop slightly below zero at lower temperatures which is caused by changes in the basis spectra as NAD freezes.

Figure 3.4 is representative of all of the measurements taken in this region of the phase diagram. In all cases, NAD was the only crystalline hydrate to be observed. At lower temperatures, it was found that no crystal formation was observed at all. It is assumed this is due to increased liquid viscosity which leads to glass formation rather than crystallization.

3.5 0.25-0.33 Mole Fraction Aerosols

As shown in figure 3.6, NAD was the first hydrate to form for most of this concentration range. However, NAT was also present as a minor constituent, increasing in importance in the region of 0.25 mole fraction. For the sample shown in figure 3.6, the amount of NAT is negligible at the freezing temperature, and rises to only 10% even at its highest recorded value.

The nitric acid phase diagram (figure 3.1) indicates that NAT should be the most stable phase in this region, and indeed, common sense would indicate that a crystalline hydrate with a composition almost exactly that of the liquid surrounding it would be more

likely to form. This however, is not the case for these measurements. Indeed, it seems clear that the barrier for nucleation of NAT is much greater than that for NAD formation.

3.6 The Effects of Annealing the Samples

Figure 3.7 shows the effect of annealing 0.25 mole fraction aerosols. Figure 3.7a was recorded as part of the experiments detailed herein while Figure 3.7b was obtained by an analysis of data published earlier.[19] Both figures represent aerosols with a mole fraction of 0.25 HNO_3. The sample shown in figure 3.7b was annealed (warmed to promote crystal growth) at about 188K, while the sample shown in 3.6a was not annealed. Note that in 3.7a, NAD is as prevalent as NAT at temperatures just below the onset of freezing, while in 3.7b, very little NAD formation is observed. In both cases, however, there is a detectable amount of NAD formed.

Clearly NAT crystals grew much more quickly than NAD crystals in this sample, particularly when it was annealed. However, the question remains as to which species is forms the nucleus. This question will be addressed below.

3.7 Kinetic Phase Diagram

Figure 3.8 shows the temperatures of the onset of freezing from plots such as 3.4 and 3.5, which are represented as circles. The results of previous studies conducted with the same experimental apparatus[18,19] are represented by squares. The bulk phase diagram is shown above for reference. Note that the maximum of the kinetic phase diagram occurs at about 0.33 mole faction, and that the temperature decreases at concentrations less than 0.25 mole fraction.

The freezing onset temperatures recorded for 0.2 μm aerosols is between 60 K and 85 K lower than that which is observed for bulk samples. It is also apparent from

comparison of the equilibrium and kinetic phase diagrams, that the behaviour of submicron nitric acid aerosols is significantly different from bulk nitric acid samples.

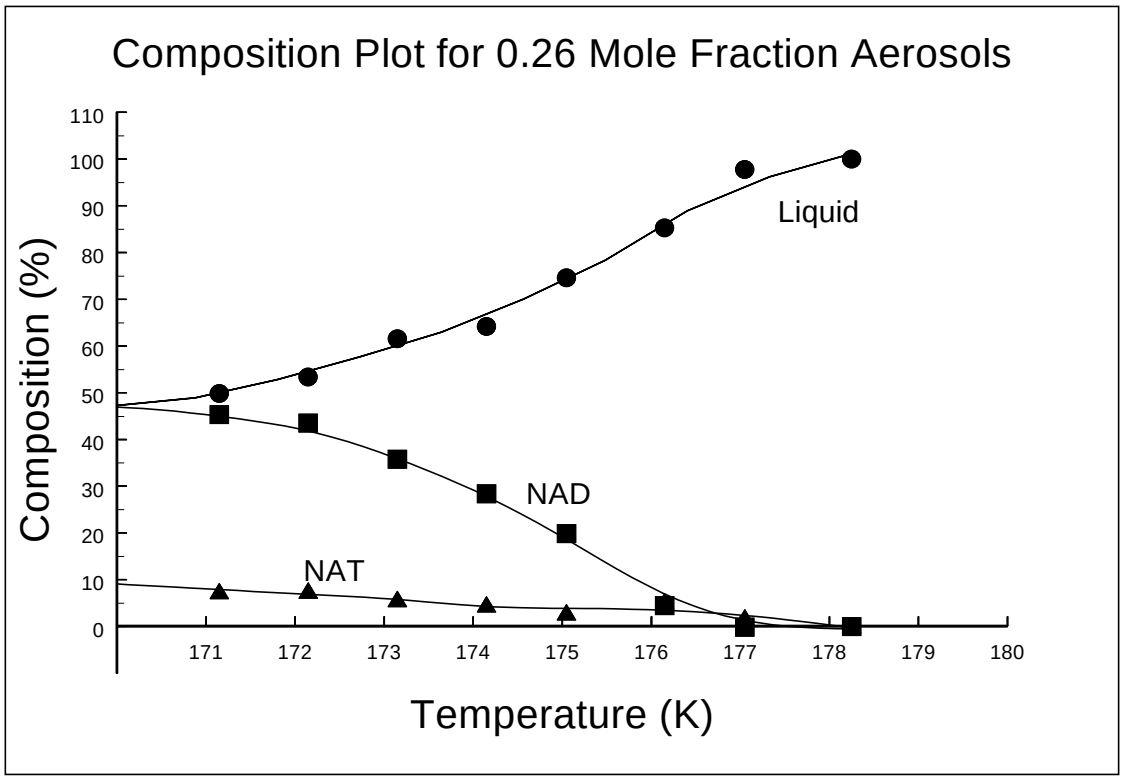

Figure 3.6
Aerosol composition as a function of temperature during freezing process for 0.26 mole fraction HNO_3 aerosols

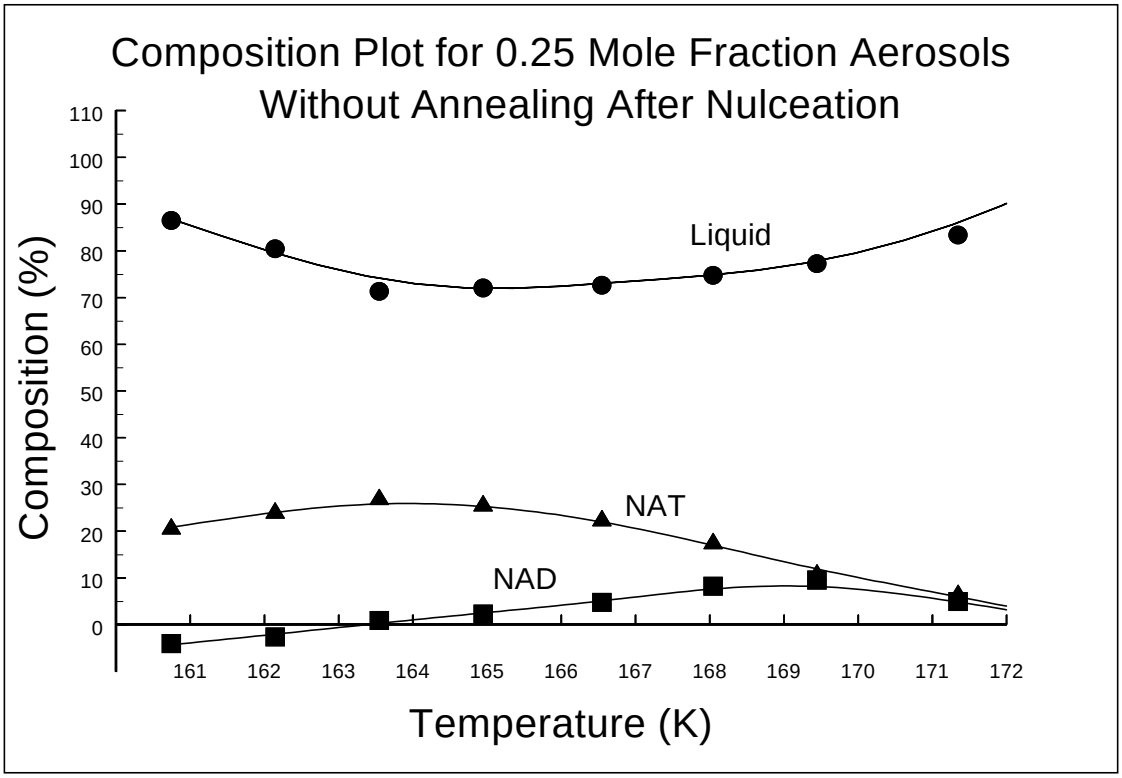

Figure 3.7a
Aerosol composition as a function of temperature during freezing process for 0.25 mole fraction HNO_3 aerosols where a 2 stage temperature profile was used

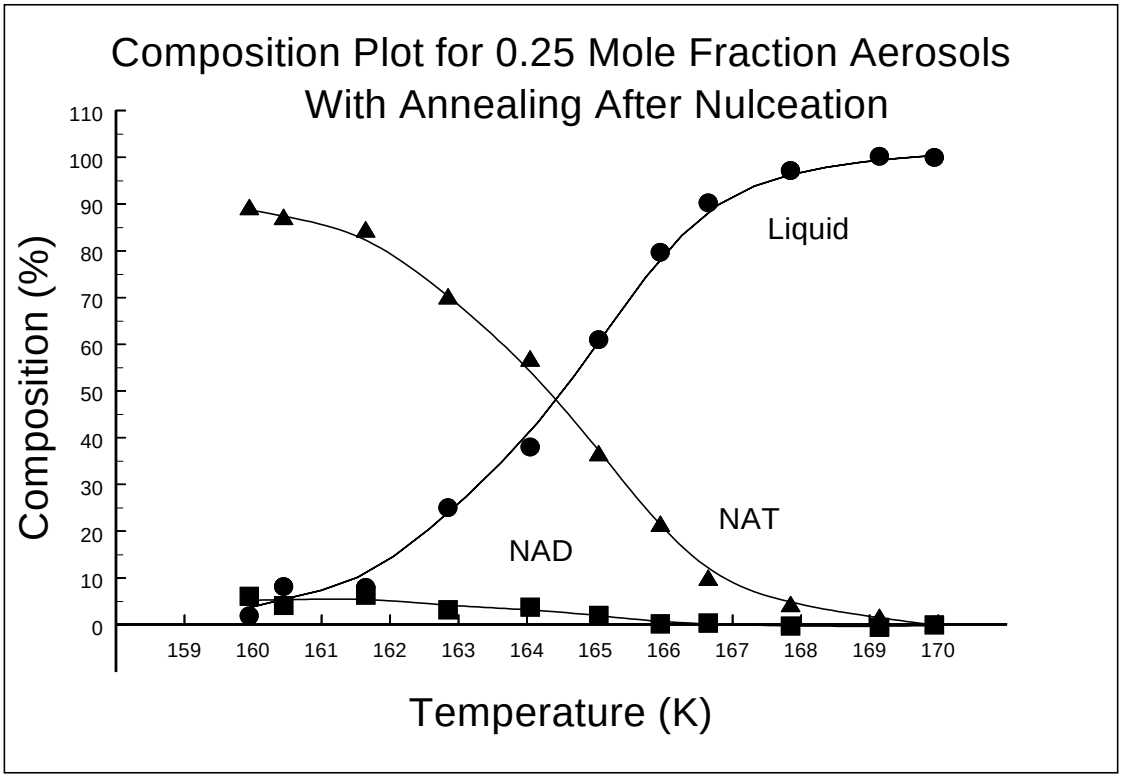

Figure 3.7b
Aerosol composition as a function of Temperature during freezing process for 0.25 mole fraction HNO_3 aerosols where aerosols were annealed at 188 K

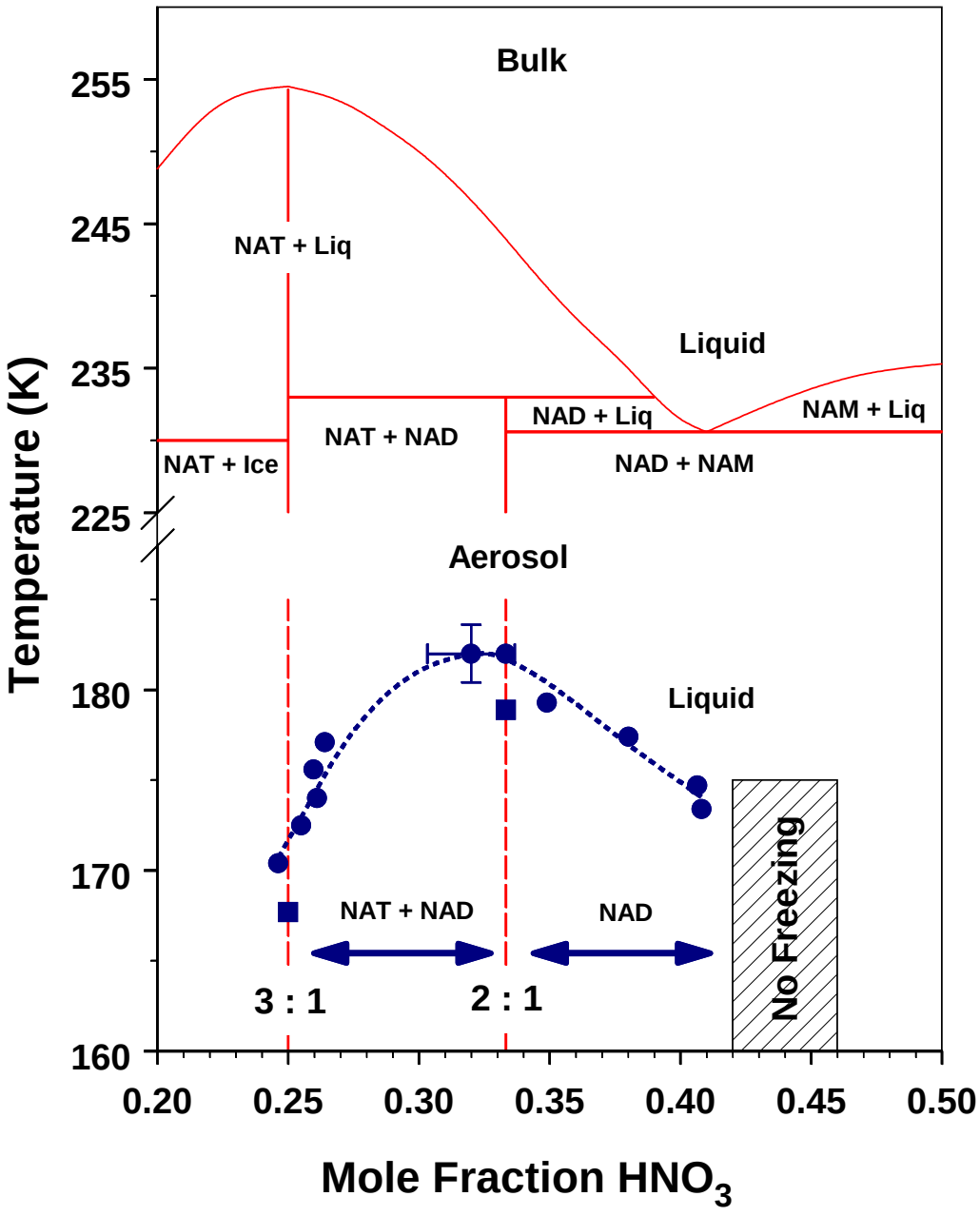

Figure 3.8
Kinetic phase diagram showing freezing temperatures of HNO_3/H_2O aerosols overlaid with bulk freezing diagram from Figure 3.1
Sample error bars are representitive of all data points.

3.8 Implications and Discussion for 0.25-0.46 Mole Fraction Aerosols

One will note from figure 3.6 that the freezing temperatures recorded in earlier work were lower than those included in this data set. It is believed that the reason for this is a variation of particle size. Classical nucleation theory tells us that the nucleation rate is proportional to the exponential of the cube of the particle radius as shown in equation 3.1.

$$P = (1 - e^{-J(T)V\Delta t}) \tag{3.1}$$

In equation 3.1, P is the probability that a particle with a volume of V is frozen after a time of Δt. J is the rate constant for nucleation. This assumes that crystal growth is fast compared to the nucleation process. A consequence of equation 3.1 is that a small change in particle size can make a significant difference in the measured freezing temperature. This is an important factor to take note of however, as differences in the sizes of PSC particles will have a significant impact upon their freezing behaviour in the stratosphere as well.

As mentioned in section 3.6, it is not clear from the data presented above which hydrate nucleates. However, this information is valuable for any who wish to understand the behaviour of nitric acid aerosols under stratospheric conditions. As part of the publication of these data[34], an attempt was made to answer this question using a thermodynamic model based on the activity of NAT reported by Carslaw et al.[35] and the activity of NAD reported by Massucci et al.[36]. These calculations indicate that for the freezing measurements reported, the saturation ratio of the solution with respect to NAD, S_{NAD}, given by equation 3.1 was nearly constant at a value between 20 and 24, while there was no apparent correlation between the data and similar saturation calculations for NAD.

$$S_{NAD} = \frac{(pHNO_3)(pH_2O)}{K_{NAD}} \tag{3.2}$$

In equation 3.2, $pHNO_3$ and pH_2O are the equilibrium partial pressures of HNO_3 and H_2O over a solution with the given concentration, and K_{NAD} is the equilibrium constant for NAD. Figure 3.9 (from ref. [28]) shows the results of these activity calculations for both NAT and NAD plotted on the same graph as the data described above. These calculations indicated that it is NAD, and not NAT that nucleates for all concentrations ≥ 0.25 mole fraction.

Similar conclusions have been drawn from other experimental evidence by Prenni et al.[37] who did not observe NAT formation in aerosols with compositions between 0.33 and 0.25 mole fraction HNO_3. Formation of NAD was observed in these aerosols.

Worsnop et al.[38], who studied thin HNO_3/H_2O films, found that NAD formed first in their films, but was then converted to NAT over time.

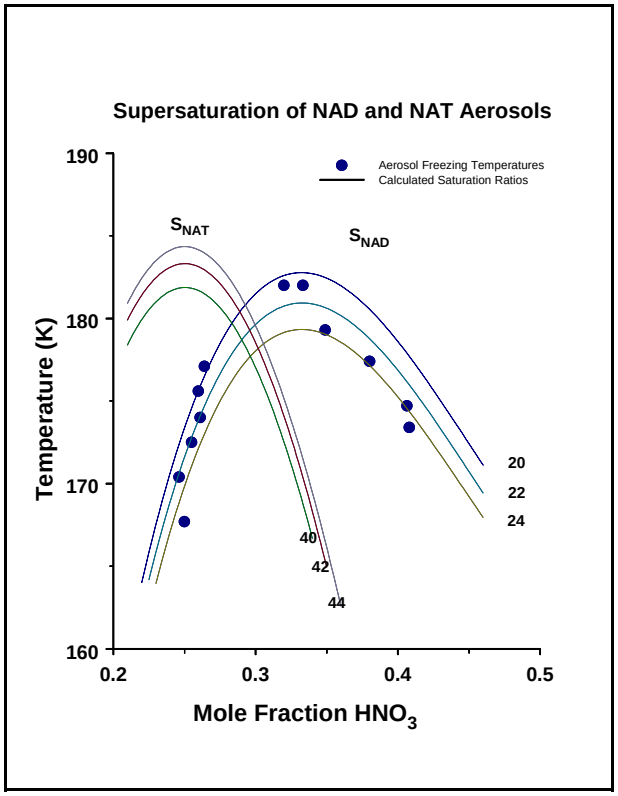

Figure 3.9
Comparison of 0.25-0.45 mole fraction HNO_3 data with saturation ratios for NAD and NAT

3.9 0-0.25 Mole Fraction Aerosols

As with the concentrated aerosols discussed previously, aerosol samples did not always crystallize completely during the residence time of aerosols in the flow tube. The focus of data analysis in this concentration range was the determination of the temperature at which crystallization was first observed. Because this concentration range displays varying physical and spectral properties, two different methods of data analysis were required in order to obtain the desired data. The first method relies on the observation of the nitrate region between 1220 cm^{-1} and 1460 cm^{-1} while the second method dealt with the OH region between 2500 cm^{-1} and 3500 cm^{-1}. Each method shall be discussed in detail below.

Figure 3.10 shows calculated spectra of liquid HNO_3/H_2O aerosols with mole fractions of HNO_3 less than 0.25. These spectra were calculated using the refractive indices of Niedziela et al.[32] and Biermann et al.[39]. Note the change in shape of the nitrate bands between 1220 cm^{-1} and 1460 cm^{-1} as the concentration changes. By examining the spectra in figure 3.10, it can be observed that the nitrate region forms two distinct peaks in the 0.10 mole fraction spectrum, while in the 0.05 mole fraction spectrum, only one peak is observed. The analysis discussed in section 3.10 (0.10-0.25 mole fraction aerosols) observes the changes in the two peaks as a function of temperature. For spectra with concentrations of HNO_3 less than 0.10 mole fraction, no changes in the nitrate region were observed during freezing. The treatment of those spectra focused on the water region between 2500 cm^{-1} and 3500 cm^{-1} . That method will be discussed in section 3.11.

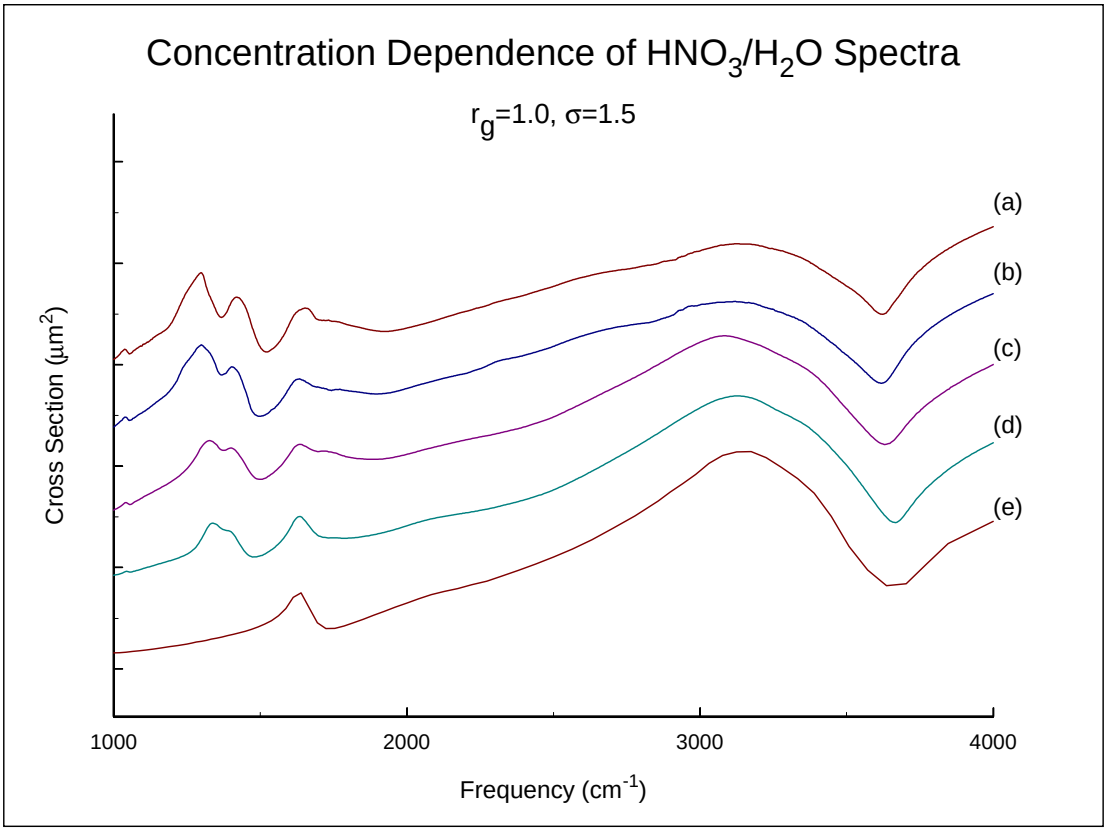

Figure 3.10
Calculated HNO_3/H_2O spectra with
r_g=1.0 and σ=1.5
(a) 0.20 mole fraction HNO_3
(b) 0.15 mole fraction HNO_3
(c) 0.10 mole fraction HNO_3
(d) 0.05 mole fraction HNO_3
(e) pure water
Optical constants:
a,b,e obtained from Niedziela et al.[32]
c,d obtained from Biermann et al.[39]

3.10 0.10-0.25 Mole Fraction Aerosols

Figure 3.11 shows the changes in the spectra of 0.11 mole fraction aerosols as a function of temperature. Note the changes in the region between 1220 cm^{-1} and 1460 cm^{-1} as the sample freezes.

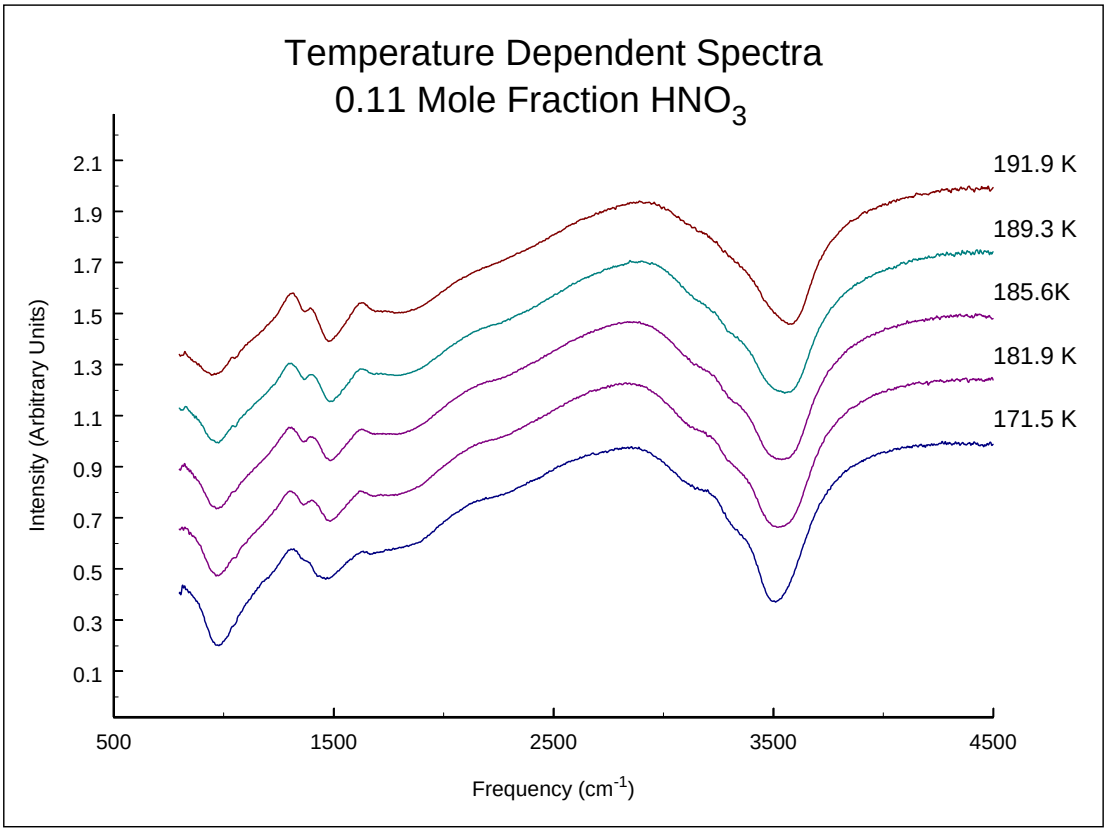

Figure 3.11
0.11 mole Fraction HNO_3 spectra as a function of temperature within the region of freezing

If we overlay the solid 0.11 mole fraction spectrum from figure 3.11 with that of NAD, NAT and Ice with comparable size distributions, as was done in figure 3.12, we see that the nitrate region is similar in character to the spectrum of NAT, and that the other crystals shown do not have similar features in that region of the spectrum.

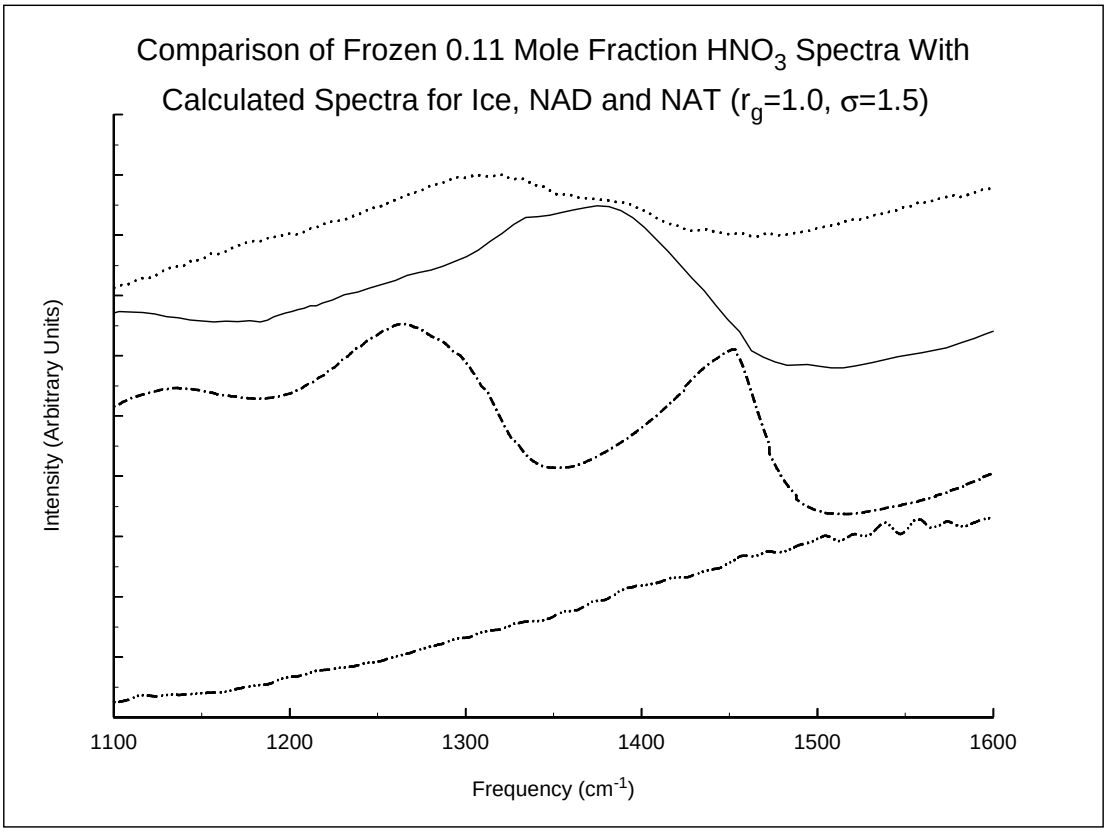

Figure 3.12
Spectra of (from top to bottom)
0.11 mole fraction HNO_3
NAT (r_g=1.0, σ=1.5)
NAD (r_g=1.0, σ=1.5)
Ice (r_g=1.0, σ=1.5)

The peaks in the region between 1220 cm^{-1} and 1460 cm^{-1} were fit to the sum of two Lorentzians and a linear baseline using a non-linear least squares fitting algorithm written by R. J. LeRoy[40]. Figure 3.13 shows the result of this fitting procedure when applied to solid and liquid 0.11 mole fraction spectra as well as NAT.

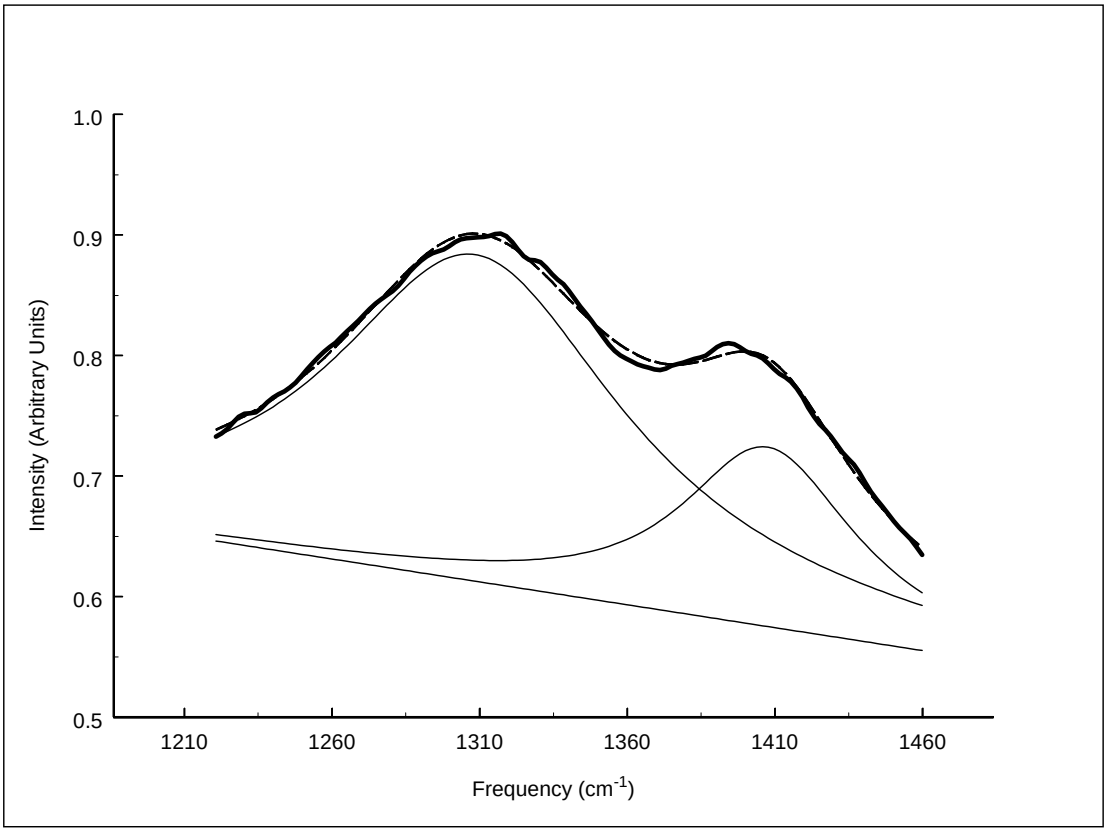

Figure 3.13a
Results of peak fitting program for liquid 0.11 mole fraction HNO_3 aerosols. The thick solid line is the input spectrum, thin solid lines are peak fitting results, and the dashed line is the sum of the Lorentzians and the baseline.

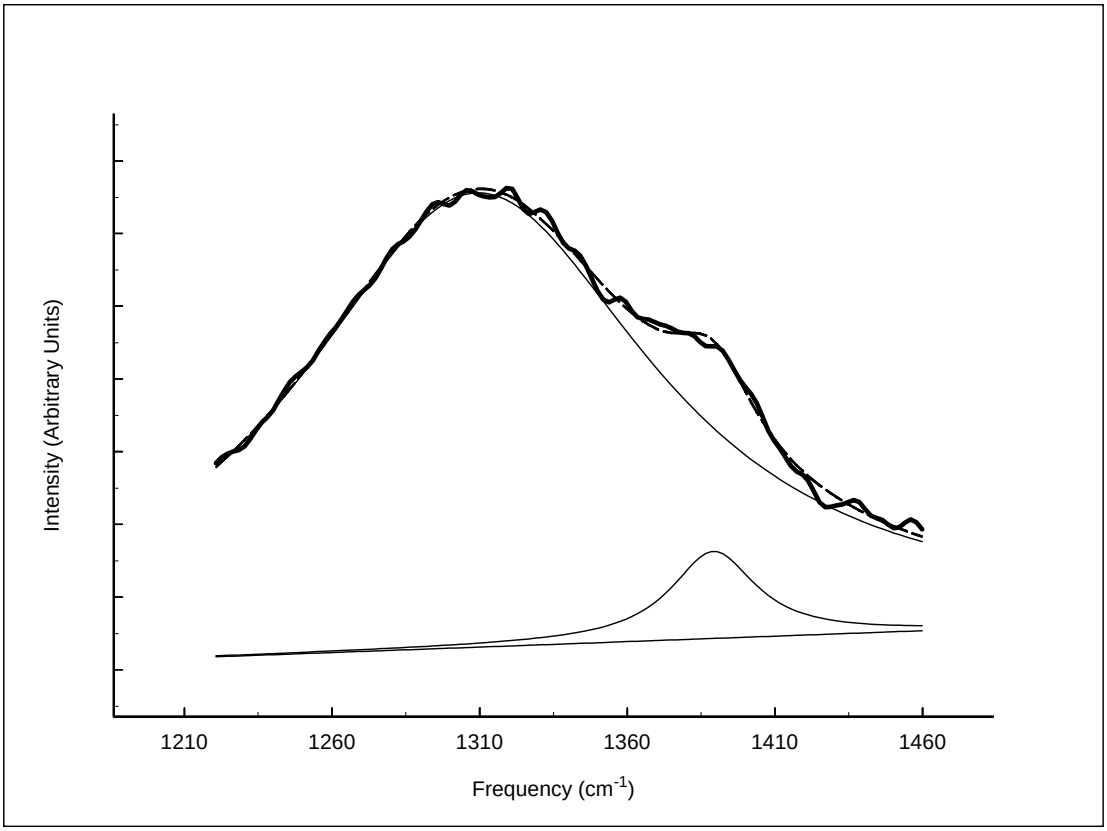

Figure 3.13b
Results of peak fitting program for partially frozen 0.11 mole fraction HNO_3 aerosols.
The thick solid line is the input spectrum, thin solid lines are peak fitting results, and the dashed line is the sum of the Lorentzians and the basline.

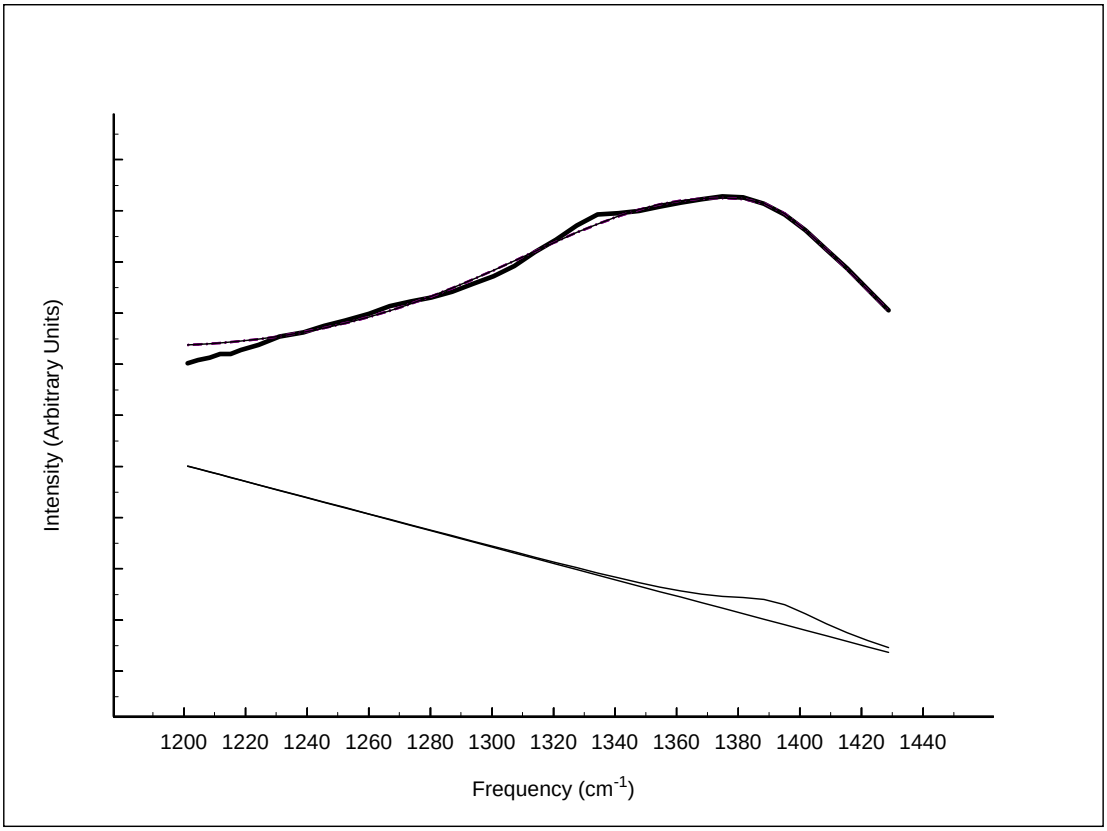

Figure 3.13c
Results of peak fitting program for NAT spectrum with r_g=1.0, σ=1.5 calculated using the optical constants of Niedziela et al.[32]
The thick solid line is the input spectrum, thin solid lines are peak fitting results, and the dashed line is the sum of the Lorentzians and the baseline.

Note that for frozen NAT, the peak at 1392 cm^{-1} is very small. The area of the peak is normalized to 100 when the sample was completely liquid. Note also the peak positions. The peak positions are shown in table 3.1. It is apparent from these that the sample shown in figure 3.13b is not completely frozen.

Material	**location of first peak**	**location of second peak**
0.11 mole fraction liquid	1308	1406
0.11 mole fraction partially frozen	1309	1390
NAT	1380	1393

Table 3.1
Locations of Lorentzian peaks found by peak fitting program

Figure 3.14 shows a comparison of the measured liquid spectra with a calculated spectrum obtained using the optical constants of Biermann et al.[39]. This is indication that the sample is completely liquid at 192 K.

The area of the high frequency peak was plotted as a function of temperature and is shown in figure 3.15. This procedure was followed for each of the samples with HNO_3 mole fraction 0.10 and greater. The temperature at which the area of the peak falls to 90 percent of its maximum value was taken as the freezing onset temperature.

The results of the analysis described above will be given in section 3.13 as the data obtained in this concentration range make more sense when considered in conjunction with the freezing temperatures for aerosols with concentrations less than 0.10 mole fraction HNO_3.

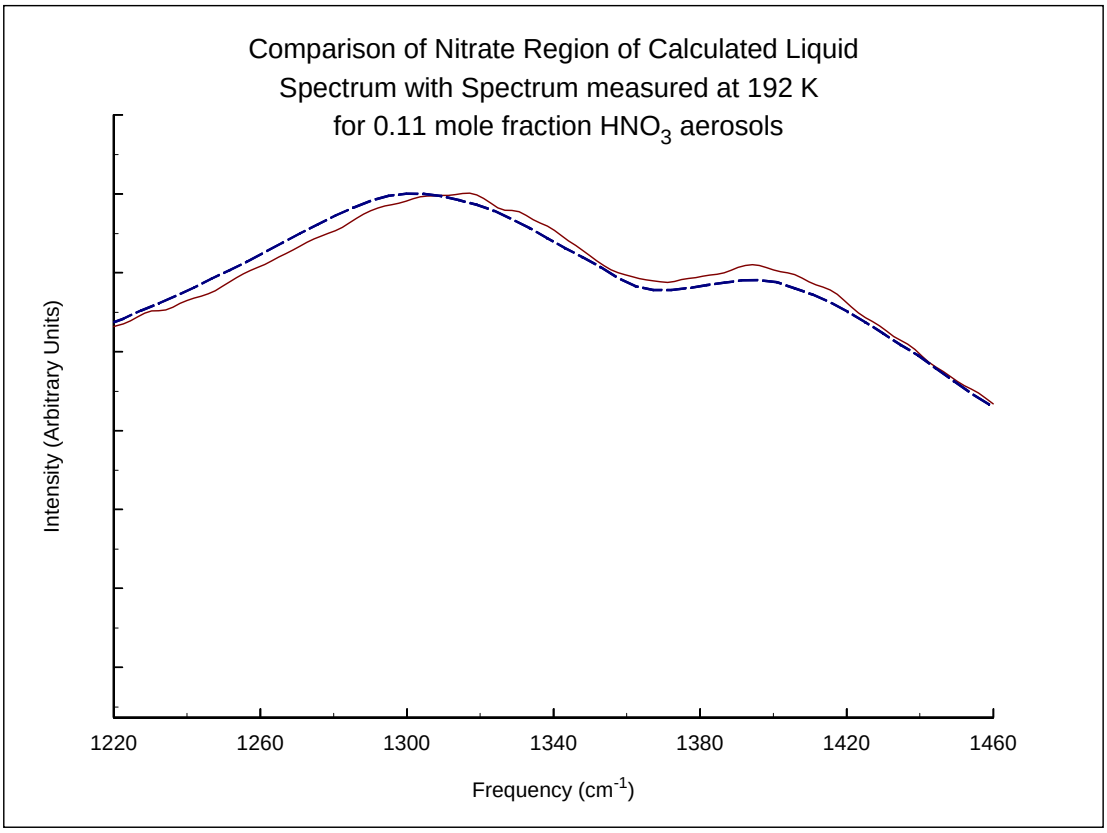

Figure 3.14
Comparison of liquid spectrum with calculated liquid spectrum optical constants supplied by Biermann et al.[39]

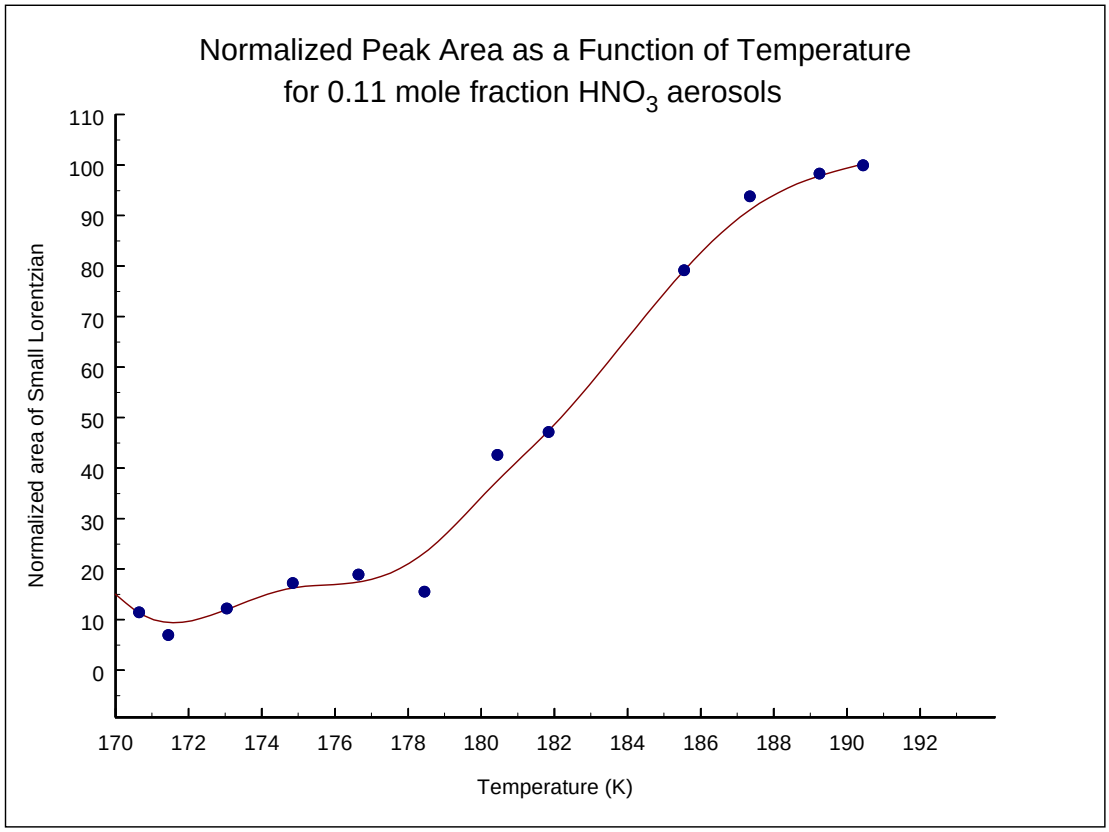

Figure 3.15
Normalized area of the 1392 cm^{-1} peak as a function of temperature

3.11 0-0.10 Mole Fraction Aerosols

Aerosol spectra with concentrations less than 0.10 mole fraction HNO_3 displayed little or no change in the nitrate region between 1220 cm^{-1} and 1460 cm^{-1}. It is therefore assumed that the crystalline substance formed is not a nitric acid hydrate, but rather water ice crystals. This is demonstrated below. Figure 3.16 shows the temperature-evolution of 0.08 mole fraction HNO_3 spectra. Note that the OH region between 2500 cm^{-1} and 3500 cm^{-1} show significant changes as a function of temperature.

The changes which take place as a function of temperature become more apparent when one subtracts the spectrum of liquid particles of the same concentration from the partially frozen spectra, as is shown in figure 3.17. Comparisons of these “difference spectra” with spectra of liquid water and ice crystals reveal much about the changes which take place in these particles. Optical constants were obtained from Niedziela et al.[32] and Kou et al.[41]

Figure 3.18 shows spectra for water and ice aerosols. It can be seen that the OH region between 2500 cm^{-1} and 3500 cm^{-1} is shifted to slightly higher frequencies for liquid water than is the case for ice. Figure 3.19 shows what the "difference" spectrum would look like for liquid water freezing to form ice. The features of the spectrum shown in figure 3.19 match those of figure 3.17 quite closely. This indicates that water is crystallizing to form ice.

The square of the intensities of the difference spectra were summed between 2500 cm^{-1} and 3500 cm^{-1} and the totals plotted as a function of temperature. The square is used so that the positive contribution from forming ice and the negative contribution from diminishing liquid water are both included. The result of this process for 0.08 mole fraction HNO_3 aerosols is shown in figure 3.20. The onset of freezing is taken as the temperature at which the area of the square of the spectrum rises to ten percent of its maximum value. These data will be discussed in greater detail in the next section.

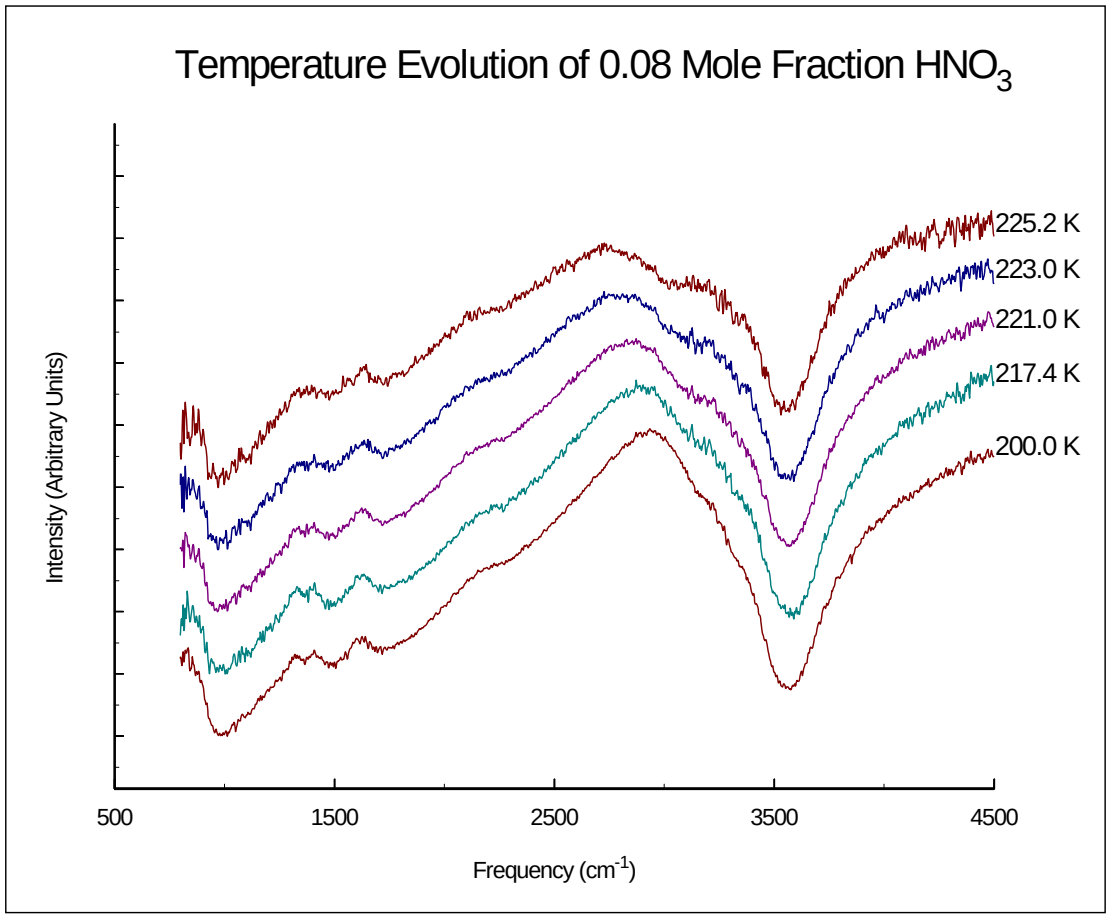

Figure 3.16
Temperature evolution of 0.08 mole fraction HNO_3 aerosols

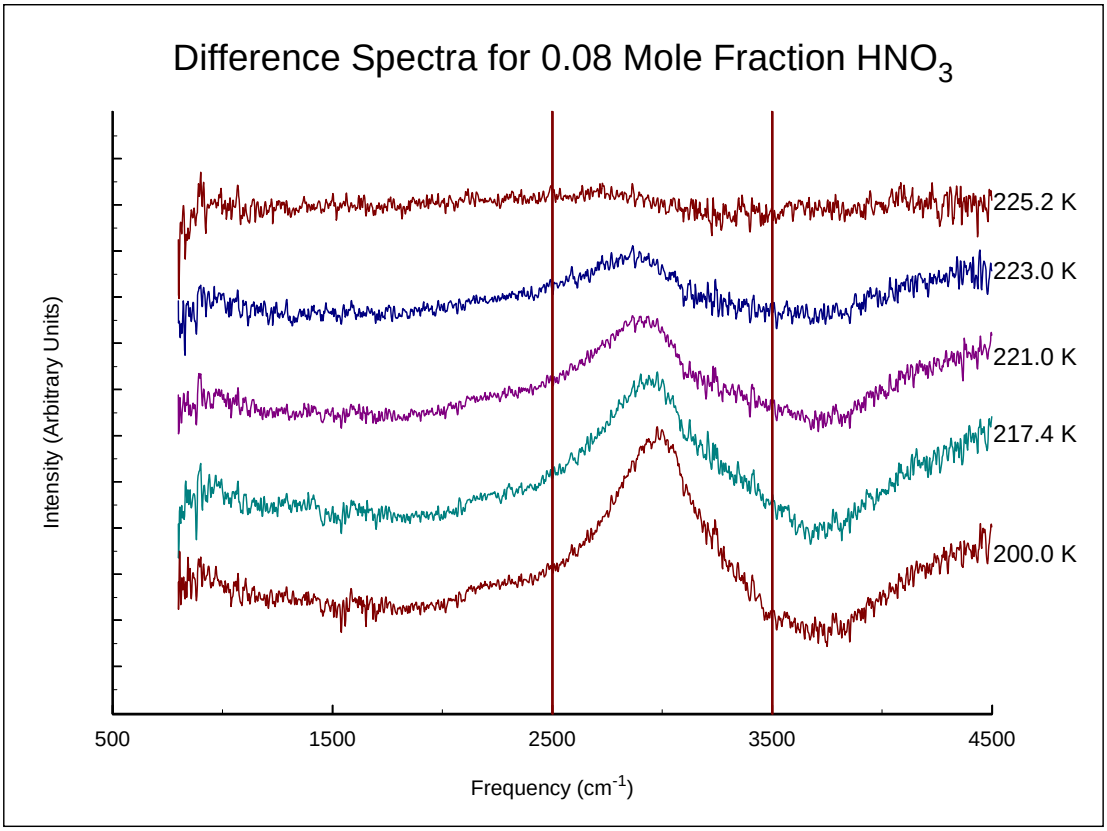

Figure 3.17
Difference spectra for 0.08 mole fraction HNO_3 as a function of temperature

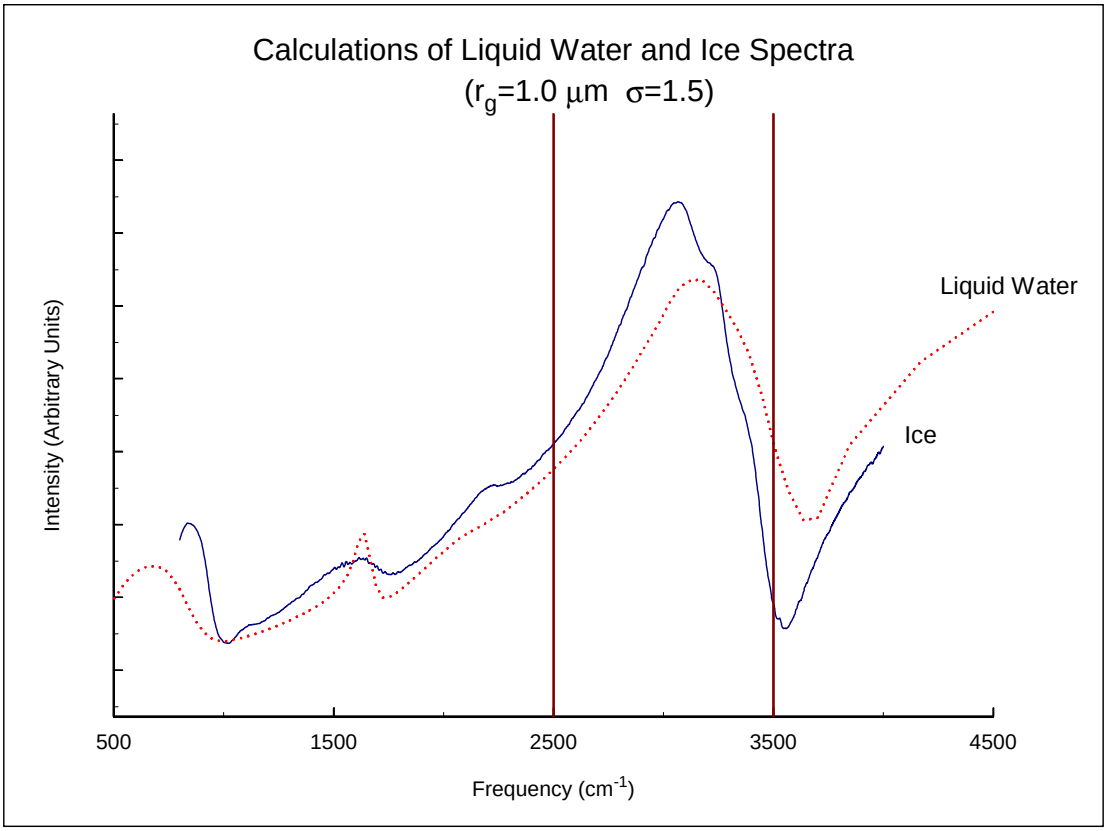

Figure 3.18
Liquid water and Ice with r_g=1.5 and σ=1.5
Ice optical constants from Niedziela et al.[32]
Water optical constants from Kou et al.[41]

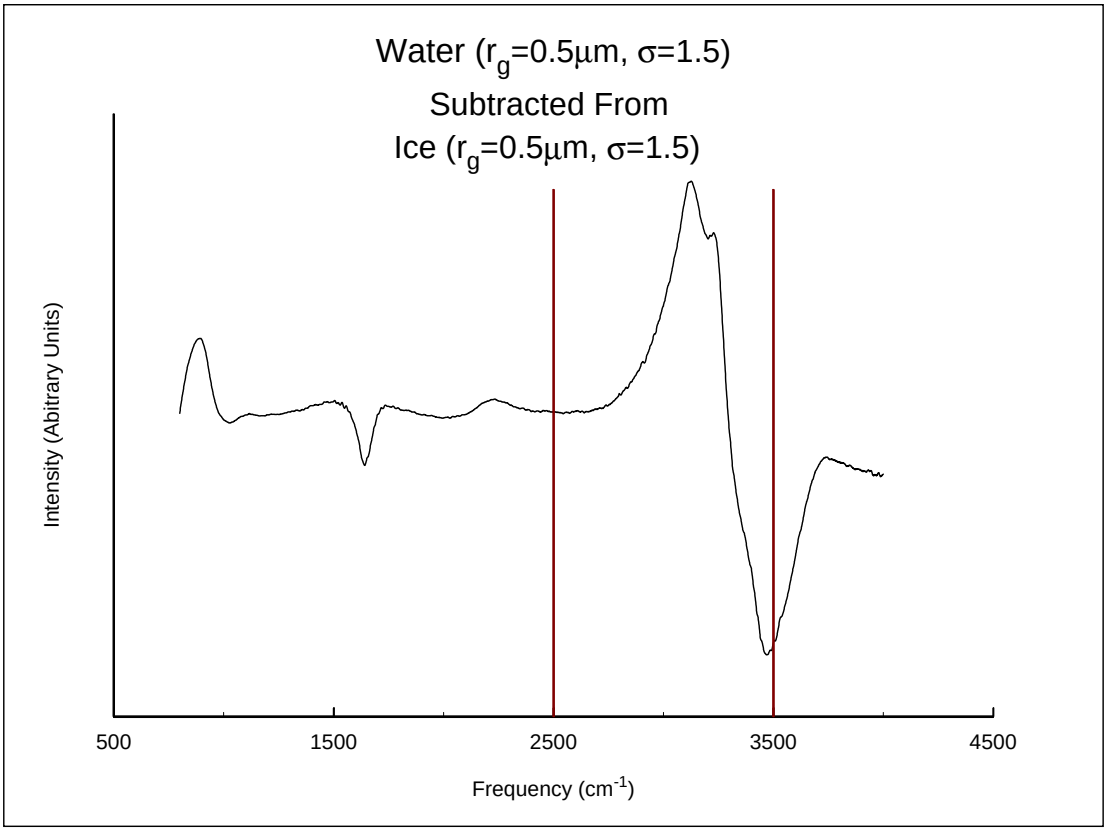

Figure 3.19
Water spectrum subtracted from ice spectrum

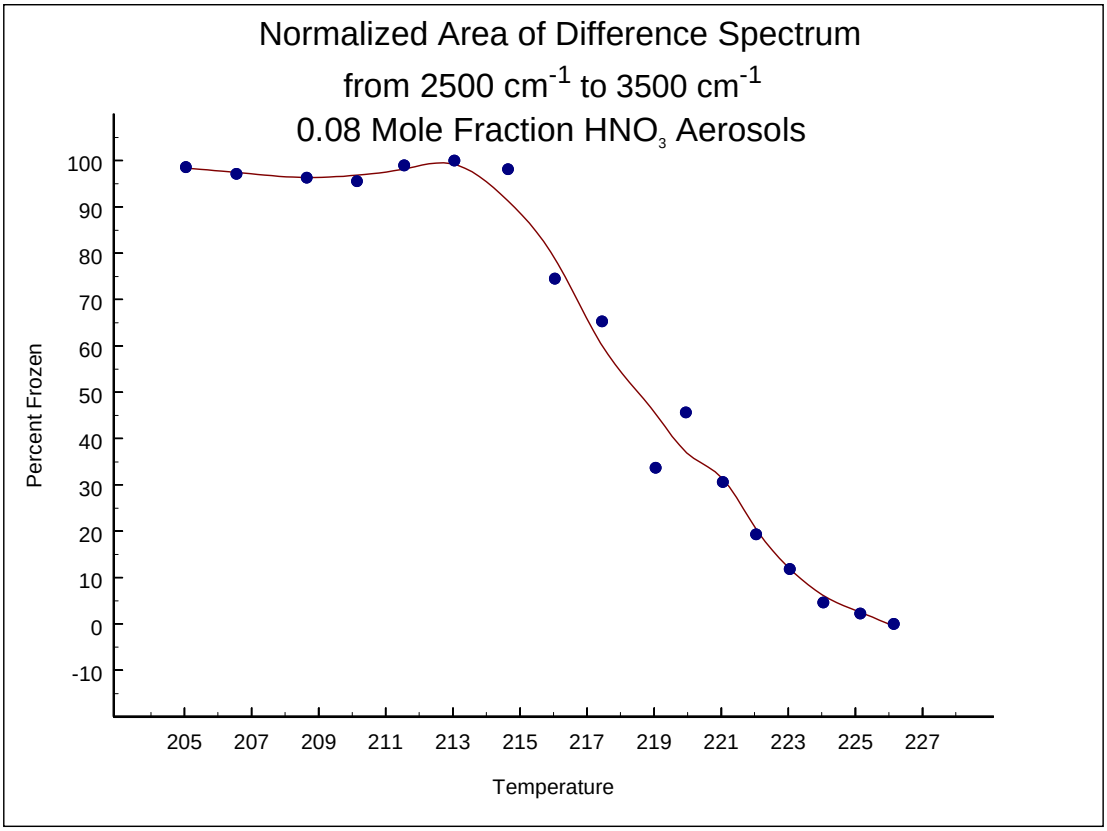

Figure 3.20
Percent Frozen as a function of temperature for 0.08 mole fraction HNO_3 aerosols

3.12 Implications and Discussion for 0-0.25 Mole Fraction Data

3.12.1 Full Kinetic Phase Diagram

The data obtained through the analysis described in the previous two sections has been incorporated into an expanded kinetic phase diagram (Figure 3.20) The fit lines shown are meant as an aid for the reader, as more points are required in several regions in order to determine the shapes of the curves with more certainty. This phase diagram does provide some indication of freezing temperature as a function of aerosol composition.

Note the two points between 0.125 and 0.25 mole fraction HNO_3, and their correspondence to the fit line generated through the data obtained for concentrations greater than 0.25 mole fraction HNO_3. As mentioned previously, the geometric mean radius of particles studied in the dilute studies were a factor of four or five larger than those described in Allan Bertram's Ph.D. thesis. This tends to indicate that the homogenous nucleation rate for nitric acid particles with compositions between 0.20 and 0.33 mole fraction HNO_3 are much more dependent on temperature than on particle size. This has important implications for modelling of cloud particles in the middle atmosphere.

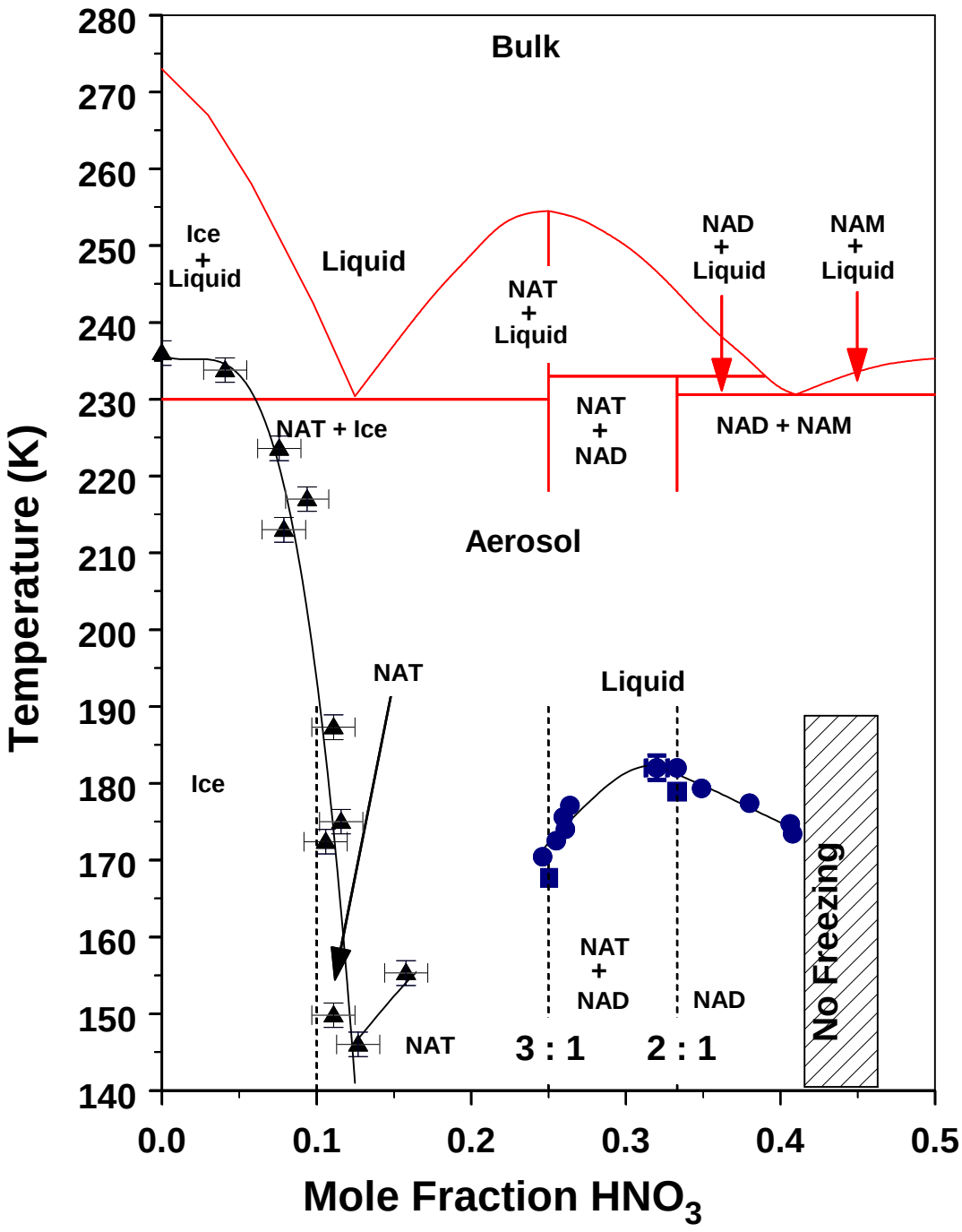

Figure 3.21
Expanded phase diagram for HNO_3/H_2O

3.12.2 Comparison with Other Data

Chang et al.[42] studied the freezing of HNO_3/H_2O droplets as well as ternary solutions containing $HNO_3/H_2SO_4/H_2O$. These studies were conducted using droplets with an average radius of approximately 2.3 μm emulsified in a mixture of halocarbon oil and lanolin.

A comparison of the data presented above with the work of Chang et al. for aerosols less concentrated than the bulk phase eutectic at 0.125 mole fraction HNO_3 is presented in figure 3.21.

There is some disagreement between the data presented here and that presented by Chang et al.. The source of this disagreement is not currently understood, and should be one of the primary aims of future work on this system.

The data presented by Chang et al. were obtained using differential scanning calorimetry, and the temperatures recorded are for ninety percent of the sample being frozen. While this difference would be expected to explain some discrepancy between the two results, it seems unlikely that this alone would account for such large differences in temperature. (The freezing point ranges encountered in our data were between ten and fifteen Kelvin.) The data presented by Chang et al. is for aerosols which were not annealed. Nucleation and crystal growth were conducted at the same temperature. Perhaps nucleation is occurring at a much lower temperature than that at which freezing is observed. Without more experiments into this matter, however, it is not clear how significant of an effect this would have on the freezing temperatures reported.

Chang et al. also report that no crystallization was observed aerosols between 0.16 and 0.40 mole fraction HNO_3. Freezing processes for aerosols in this concentration range are well documented however.[18,19,34,43] Chang et al. note this disagreement but are unable to offer an explanation.

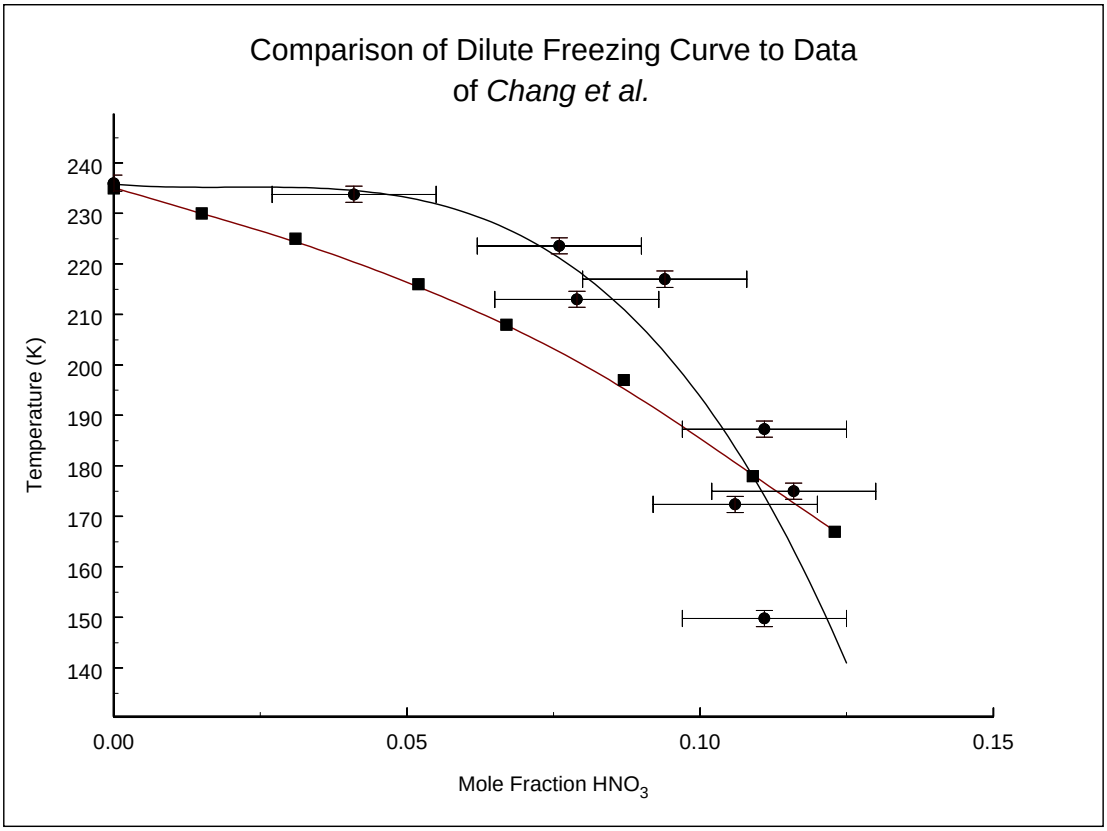

Figure 3.22
Comparison of the work described in this thesis (circles) to the work of Chang et al. (squares)

3.13 Future Work

The work on the HNO_3/H_2O system is not yet complete. More data is needed in order to determine the shape of the curve between 0.125 and 0.25 mole fraction with more certainty. More work is also needed in order to determine which species are responsible for nucleation in HNO_3/H_2O aerosols with compositions less than 0.25 mole fraction HNO_3. This will entail suitable saturation calculations such as those mentioned in section 3.8.

An explanation is needed for the discrepancies between the work presented in this thesis and the work presented by Chang et al..

Ternary $HNO_3/H_2SO_4/H_2O$ aerosols should be studied using the methods described in this thesis, as these aerosols are more similar in composition to what is expected to occur in the lower stratosphere. This data should be compared with data obtained from thin film and emulsion data and any differences explained.

Although our knowledge of the freezing kinetics of the materials which compose the middle atmosphere is growing, there is still much more work that needs to be in order to be able to create useful models of this system.

References

[1] J.H. Seinfeld, S.N. Pandis, *"Atmospheric Chemistry and Physics - From Air Pollution to Climate Change"*, 164-171, John Wiley & Sons, Inc.,(1998)

[2]M.J. Molina, and F.S. Rowland, "Stratospheric sink for chlorofluoromethanes. Chlorine atom-catalyzed destruction of ozone", *Nature*, **249**, 810-812, (1974)

[3] P.J. Wooldridge, R. Zhang, and J.J. Moline, "Phase equilibria of H_2SO_4, HNO_3, and HCl hydrates and the composition of polar stratospheric clouds", *J. Geophys. Res.*, **102**, 10777-10784 (1997)

[4] S.E. Anthony et al., "Laboratory studies of ternary $H_2SO_4/HNO_3/H_2O$ particles: Implications for polar stratospheric cloud formation", *J. Geophys. Res.*, **102**, 10777-10784, (1997)

[5] E.V. Browell et al., "Airborn Lidar Observations in the Wintertime Arctic Stratosphere: Polar Stratospheric Clouds", *Geophys. Res. Lett.*, **17**, 385-388, (1990)

[6] T. Peter, "Microphysics and Heterogeneous Chemistry of Polar Stratospheric Clouds", *Annu. Rev. Phys. Chem.* **48**, 785-822, (1997)

[7] C.R. Webster et al., "Chlorine Chemistry on Polar Stratospheric Cloud Particles in the Arctic Winter", *Science*, **261**, 1130-1133, (1993)

[8] J.M. Van Doren et al., "Uptake of N_2O_5 and HNO_3 by Aqueous Sulfuric Acid Droplets", *J. Phys. Chem.*, **95**, 1684-1689, (1991)

[9] R.L. Jones et al., "The polar stratospheric cloud event of January 24: Part 2, photochemistry", *Geophys. Res. Lett.*, 17, suppl. 541-544, 1990

[10] J. Sessler, P.Good, A.R. MacKenzie, and J.A. Pyle, "What role do type I polar stratospheric cloud and aerosol parameterizations play in modeled lower stratospheric chlorine activation and ozone loss?", *J. Geophys. Res.*, **101**, 28,871-28,835, (1996)

[11]K.S. Carslaw et al., "Partles microphysics and chemistry in remotely observed mountain polar stratospheric clouds", *J. Geophys. Res.*, **103**, 5785-5796, (1998)

[12] Larsen, N., J.M. Rosen, N.T. Kjome, and B. Knudsen, "Deliquescence and freezing of stratospheric aerosol observed by balloonborne backscattersondes", *Geophys. Res. Lett.*, **22**, 1233-1236, (1995)

[13] H.R. Pruppacher, "A New Look at Homogeneous Ice Nucleation in Supercooled Water Drops", *Journal of the Atmospheric Sciences*, **52**, 1924-1933, (1995)

[14] U.M.Biermann, P.J. Crutzen, and T. Peter, “The Unsuitablilty of Meteoritic and other nuclei for polar stratospheric cloud freezing”, *Geophys. Res. Lett.*, **23**, 1693-1696, (1996)

[15] H. Rawson, *Properties and Applications of Glass*, 1-17, Elsevier Scientific Publishing company, (1980)

[16] H. Scholze, *Glass Nature, Structure and Properties*, 56-69, Springer-Verlag, (1990)

[17] D. Turnbull, and M.H. Cohen, “Concerning Reconstructive Transformation and Formation of Glass”, *J. Chem. Phys.*, **29**, 1049-1054, (1958)

[18] A.K. Bertram, and J.J. Sloan, “Temperature-dependant nucleation rate constants and freezing behavior of submicron nitric acid dihydrate particles under stratospheric conditions”, *H. Geophys. Res.*,**103**, 3553-3561, (1998)

[19] A.K. Bertram, J.J. Sloan, “The nucleation rate constants and freezing mechanism of nitric acid trihydrate aerosol under stratospheric conditions”, *J. Geophys. Res.*, **103**, 13261-13265, (1998)

[20] A.K. Bertram, PhD. Thesis, *University of Waterloo*, (1998)

[21]C.F. Bohren, and D.R. HUffman, *Absorption and Scattering of Light by Small Particles*, John Wiley & Sons, (1993)

[22]P.C. Reist, *Aerosol Science and Technology*, 13-25, McGraw-Hill, Inc, (1993)

[23]W.H. Press, B.P. Flannery, S.A. Teukolsky, and W.T. Vetterling, *Numerical Recipes - The Art of Scientific Computing (FORTRAN Version)*, Cambridge University Press, (1989)

[24]B.T. Draine, and P.J. Flatau, "Discrete dipole approximation for scattering calculations", *J. Opt. Soc. Am.*, **A11**, 1491, (1994)

[25]A.C. Holland and J.S. Draper, “Analytical and Experimental Investigation of Light Scattering from Polydispersions of Mie Particles”, *Appl. Opt.*, **6**, (1967)

[26]R.J. Perry, A.J. Hunt, D.R. Huffman, “Experimental determinations of Meuller scattering matrices for nonspherical particles”, *Appl. Opt.*, **17**, (1978)

[27]P. Atkins *Physical Chemistry fifth edition*, 824, W.H. Freeman and Company, (1994)

[28]D.E. Taleb et al., "Vapour pressures in the ternary system water-nitric acid-sulfuric acid at low temperature: A reexamination", *J. Geophys. Res.*, **101**, 25967-25977, (1996)

[29]A.J. Baran, J.S. Foot, and D.L. Mitchell, "Ice-crystal absorption: a comparison between theory and implications for remote sensing", *Appl. Opt.*, **37**, 2207-2215, (1998)

[30]R.C. Weast, S. M. Selby, C.D. Hodgman, CRC handbook of Chemistry and Physics forty-sixth edition, Chemical Rubber Co., (1965)

[31]N. Barton, B. Rowland, and J.P. Devlin, "Infrared spectra of large acid hydrate clusters: Formation conditions of submicron particles of nitric acid dihydrate and trihydrate." *J. Phys. Chem.*, **97**, 5848-5851, (1993)

[32]R.F. Niedziela, R.E. Miller, and D.R. Worsnop, "Temperature- and frequency-dependent optical constants for nitric acid dihydrate from aerosol spectroscopy", *J. Phys. Chem. A*, **102**, 6477-6484, (1998)

[33]B.G. Koehler, A.M. Middlebrook, and M.A. Tolbert, "Characterization of model polar stratospheric cloud films using Fourier transform infrared spectroscopy and temperature programmed desorption", *J. Geophys. Res.*, **97**, 8065-8074, (1992)

[34]A.K. Bertram, D.B. Dickens, and J.J. Sloan, "Supercooling of type 1 polar stratospheric clouds: The freezing of submicron nitric acid aerosols having HNO_3 mol fractions less than 0.5", *J. Geophys. Res.*, **105**, 9283-9290, (2000)

[35]K.S. Carslaw et al., "Stratospheric aerosol growth and HNO_3 gas phase depletion from coupled HNO_3 and water uptake by liquid particles", *Geophys. Res. Lett.*, **21**, 2479-2482, (1994)

[36]M. Massucci, S.L. Clegg, and P. Brimblecombe, "Equilibrium partial pressures, thermodynamic properties of aqueous and solid phases, and Cl_2 production from aqueous HCl and HNO_3 and their mixtures", *J. Phys. Chem. A*, **103**, 4209-4266, (1999)

[37]A.J. Prenni et al., "Composition dependent freezing nucleation rates for HNO_3/H_2O aerosols resembling gravity wave perturbed stratospheric particles, *J. Geophys. Res.*, **103**, 28439-28450, (1998)

[38]D.R. Worsnop et al., "Vapour pressures of solid hydrates of nitric acid: Implications for polar stratospheric clouds", *Science*, **259**, 71-74, (1993)

[39]U.M. Biermann, B.P. Luo, and Th. Peter, "Absorption Spectra and Optical Constants of Binary and Ternary Solutions of H_2SO_4, HNO_3, and H_2O in the Mid Infrared at Atmospheric Temperatures", *J. Phys. Chem. A*, **104**, 783-793, (2000)

[40]R.J. LeRoy, *University of Waterloo*, Private communication

[41]L.Kou, D.Labrie, P.Chylek, “Refractive indices of water and ice in the 0.65 to 2.5 micron range”, *Appl. Opt.*, **32**, 3531-3540, (1993)

[42]H.A. Chang et al.,"Phase Transitions in Emulsified HNO_3/H_2O and $HNO_3H_2SO_4/H_2O$ Solutions", *J. Phys. Chem. A*, **103**, 2673-2679, (1999)

[43]A. Tsias et al.,"Freezing of polar stratospheric clouds in orographically induced strong warming events", *Geophys. Res. Lett.*, **24**, 2303-2306, (1997)